THE ASTRONOMICAL JOURNAL, 121:182–197, 2001 January

HUBBLE SPACE TELESCOPE OBSERVATIONS OF DUST AND STAR-FORMING REGIONS IN THE OCULAR GALAXY IC 2163 AND ITS SPIRAL COMPANION NGC 2207

DEBRA MELOY ELMEGREEN,[1] MICHELE KAUFMAN,[2] BRUCE G. ELMEGREEN,[3] ELIAS BRINKS,[4] CURTIS STRUCK,[5] MARIO KLARIĆ,[6] AND MAGNUS THOMASSON[7]

Received 2000 August 16; accepted 2000 October 3

ABSTRACT

Hubble Space Telescope observations in *U*, *B*, *V*, and *I* passbands of the interacting spiral galaxies IC 2163 and NGC 2207 are used to measure extinctions in the cloud and intercloud regions and ages and luminosities of the star-forming regions. The extinction in the part of NGC 2207 seen in projection against IC 2163 was determined by using the method of White & Keel. The extinctions there and elsewhere were also determined from radiative transfer models of the magnitude differences between clouds and their surroundings. The intercloud extinction in *V* band ranges from 0.5 to 1 mag on the line of sight, and the cloud extinction ranges from 1 to 2 mag. The measured star-forming regions in these galaxies have a power-law relation between size and luminosity and a power-law luminosity distribution function. These power laws are consistent with a fractal dimension for the star formation that is the same as that for interstellar gas, $D \sim 2.2$, extending over scales ranging from 20 to 1000 pc. Fifteen compact massive star clusters that are analogous to super–star clusters found in starburst regions are in the spiral arms of NGC 2207. Nothing is peculiar about these regions except for a high H I velocity dispersion (~ 50 km s^{-1}). Two more super–star clusters are in the tidally compressed oval of IC 2163. These clusters have masses ranging from $\sim 10^4$ to 2×10^5 $M_\odot$ and ages of a few times 10^6 yr.

Key words: dust, extinction — galaxies: individual (IC 2163, NGC 2207) — galaxies: interactions — galaxies: star clusters

1. INTRODUCTION

The spiral galaxies IC 2163 and NGC 2207 are a dramatic interacting pair, with NGC 2207 in the foreground obscuring IC 2163. Ground-based observations in optical, H I, and radio continuum show evidence for the interaction in the form of tidal arms and 100 km s^{-1} streaming motions in an eye-shaped central oval of IC 2163, regions with H I velocity dispersion of up to 50 km s^{-1} in both galaxies, and a strongly warped disk in NGC 2207 (Elmegreen et al. 1995b, hereafter Paper I). The ocular (eyelike) shape is common for prograde, in-plane tidal interactions (Sundin 1989, 215; Elmegreen et al. 1991; Donner, Engstrom, & Sundelius 1991). Computer simulations reproduce the main kinematical and morphological features of this interacting pair, suggesting that perigalacticon occurred 4×10^7 yr ago as IC 2163 passed behind NGC 2207 from west to east (Elmegreen et al. 1995a, hereafter Paper II; Elmegreen et al. 2000b, hereafter Paper III).

The purpose of the present paper is to use *Hubble Space Telescope* (*HST*) observations in *U*, *B*, *V*, and *I* passbands to study the distribution of dust and star formation in these galaxies. Ground-based Hα images (D. A. Hunter 1999, private communication) provide a complementary view on a larger scale. The peculiar morphological features that are revealed by the *HST* images were discussed in Paper III, including filamentary dust spirals with embedded young stars in NGC 2207, filamentary dust in the tidal arm of IC 2163, emission streaks several hundred parsecs long in both galaxies, and a luminous star-forming region with a dark conical cloud 400 pc long in the far west of NGC 2207. Some of the properties of these features are measured here. Unusual dust spirals in the nucleus of NGC 2207 were discussed by Elmegreen et al. (1998).

One of the most interesting aspects of these galaxies is that NGC 2207 is seen in projection toward IC 2163, which allows a determination of the extinction in the foreground galaxy. Internal galaxy extinction is usually difficult to measure. Disney, Davies, & Phillipps (1989) and Valentijn (1990) used inclination statistics to deduce that spiral disks are largely opaque. This result was controversial, so White & Keel (1992) developed a direct photometry method to measure disk opacity using partially overlapping galaxy pairs. This method has been applied to several nearly face-on spiral galaxies with the conclusions that spiral arms can be optically thick but interarm regions are nearly transparent (White & Keel 1992; White, Keel, & Conselice 1996, 214; Berlind et al. 1997; Rönnback & Shaver 1997; Domingue, Keel, & White 2000; White, Keel, & Conselice 2000).

Berlind et al. (1997) applied the White & Keel method to ground-based images of NGC 2207 and derived 1–2 mag of visual extinction through the part of the disk that is backlit by IC 2163. One of the purposes of the current paper is to review the ground-based results by Berlind et al. in the light of our much higher resolution *HST* observations by measuring extinction on scales of 34 to 85 pc.

The second topic of this paper deals with star formation in this interacting system. In nearby spiral galaxies, star

[1] Department of Physics and Astronomy, Vassar College, Poughkeepsie, NY 12604; elmegreen@vassar.edu.
[2] Department of Physics and Department of Astronomy, Ohio State University, 174 West 18th Avenue, Columbus, OH 43210-1173; rallis@mps.ohio-state.edu.
[3] IBM Research Division, T. J. Watson Research Center, P.O. Box 218, Yorktown Heights, NY 10598; bge@watson.ibm.com.
[4] Departamento de Astronomía, Universidad de Guanajuato, Apdo. Postal 144, Guanajuato, Gto. 36000, México; ebrinks@astro.ugto.mx.
[5] Department of Physics and Astronomy, Iowa State University, Ames, IA 50010; curt@iastate.edu.
[6] Columbia, SC 29202; mariok@bellsouth.net.
[7] Onsala Space Observatory, S-439 92 Onsala, Sweden; magnus@oso.chalmers.se.

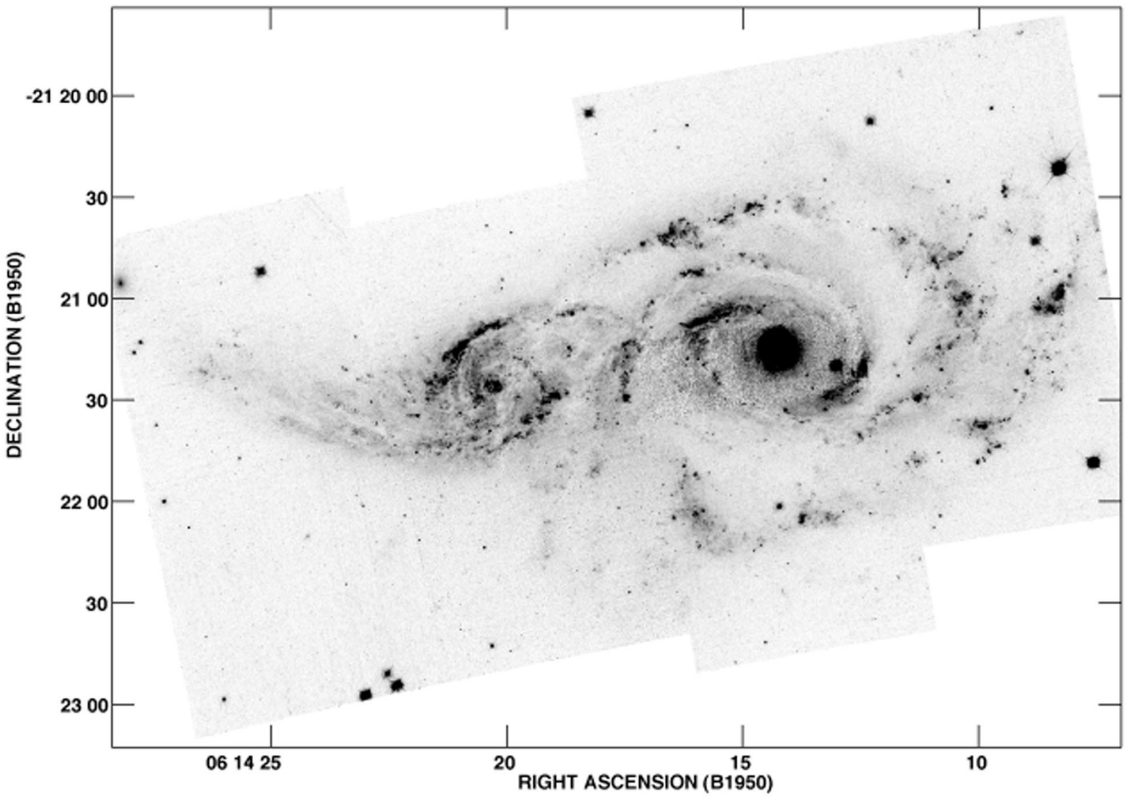

FIG. 1.—*B*-band WF mosaic of IC 2163 and NGC 2207 made from three *HST* pointings, with coordinates overlaid for reference

formation can be seen over a wide range of scales, from bound clusters to subgroups in associations, to associations and complexes that may extend for a kiloparsec (Blaauw 1964; Efremov 1995; Hodge 1986; Kennicutt & Hodge 1980; Elmegreen 1996, 1997, and others). The luminosity distribution function for star formation usually has no characteristic scale, but is a power law of the form $\sim(L^{-1})\,d\log L$ (Kennicutt, Edgar, & Hodge 1989; Gonzalez Delgado & Perez 1997; Elmegreen & Efremov 1997; Williams & McKee 1997; Oey & Clarke 1998; Elmegreen & Salzer 1999). We find the same power-law luminosity function for both stellar clusters and H II regions in NGC 2207 and IC 2163. We also find that the cluster luminosity scales approximately with the square of the diameter, as seen in normal spirals (Elmegreen & Salzer 1999), suggesting that the surface brightnesses of all stellar complexes are

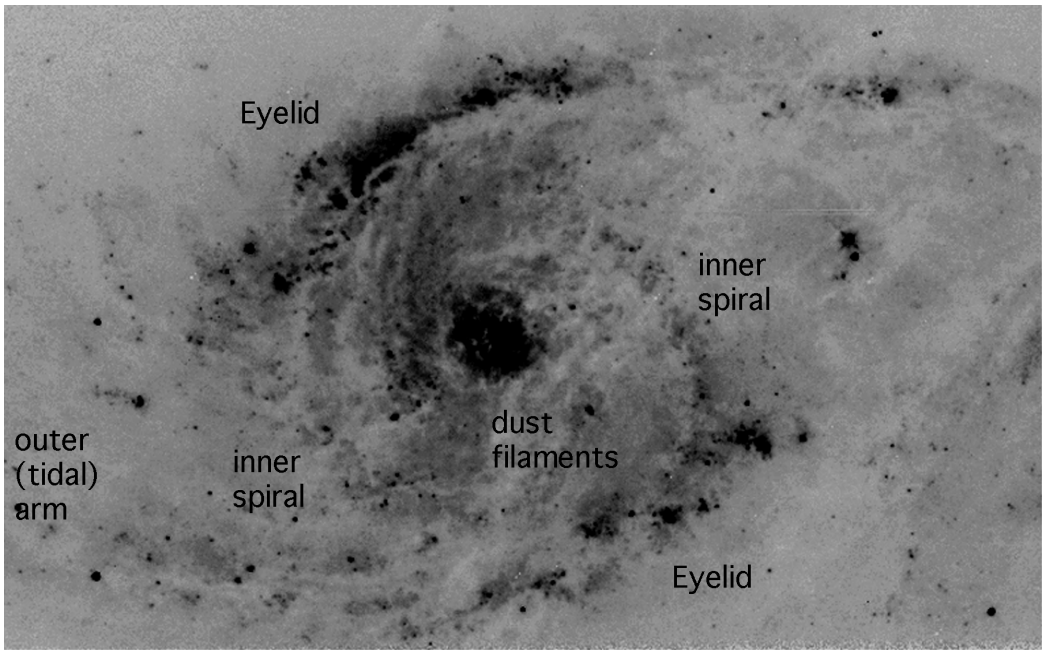

FIG. 2.—WF *V*-band image of the center of IC 2163. The field of view is 1′ wide; key features are labeled.

similar. The fractal dimension for the star-forming regions is measured from the slope of a correlation between cluster size and luminosity. The result is about the same for our regions as for the fractal dimension for interstellar gas in the Milky Way (e.g., Pfenniger & Combes 1994; Elmegreen & Falgarone 1996; Heithausen et al. 1998), suggesting that star formation follows the gas and the gas gets its structure from scale-free processes such as turbulence and self-gravity (Elmegreen et al. 2000a, 179).

We also find 17 dense and luminous young clusters a few times 10^6 yr old. They are similar to super–star clusters (SSCs) in other interacting galaxies, such as NGC 7252 (Miller et al. 1997) and the Antennae (Whitmore et al. 1999; Fritze-V. Alvensleben 1999), but somewhat less massive. Ages and masses are estimated for our star-forming regions and SSCs based on their colors and luminosities.

The distance to these galaxies is assumed to be 35 Mpc, based on a Hubble constant of 75 km s^{-1} Mpc^{-1} and the recession velocities in Paper I. IC 2163 is classified as an SB(rs)c pec type, and NGC 2207 is an SAB(rs)bc pec (de Vaucouleurs et al. 1991, hereafter RC3).

2. *HST* OBSERVATIONS AND DATA REDUCTION

The galaxies IC 2163 and NGC 2207 were observed with the *HST* Wide Field Planetary Camera 2 (WFPC2) in filters F336W (*U* band), F439W (*B* band), F555W (*V* band), and F814W (*I* band) in nine orbits with three separate pointings. Three orbits were obtained on 1996 May 25, and the remaining six were completed on 1998 November 11. Each field had four exposures in each band; the exposures were dithered. Individual image exposure times were 500 s in *U*, 500 s in *B*, 160 s in *V*, and 180 s in *I*, totaling 4.5 hours. The scale is 0.″0995 $pixel^{-1}$ for the wide-field (WF) images and 0.″0455 $pixel^{-1}$ for the planetary camera (PC) images. With this resolution, 1 WF pixel = 16.8 pc, 1 PC pixel = 7.7 pc, and 1″ = 170 pc at the assumed distance of 35 Mpc.

The standard pipeline reduction was used. The images were combined with algorithms to reject cosmic rays. A wide-field mosaic with a total field of view of 2935 × 1750 pixels, corresponding to 4.′87 × 2.′91, was produced in each filter. The *B*-band mosaic is shown in Figure 1. A WF *V*-band image of the center of IC 2163 is shown in Figure 2, where key features are labeled for subsequent reference. For intensity measurements, average sky backgrounds based on measurements of the outermost regions of each image were subtracted in each band.

3. EXTINCTION IN NGC 2207 AND IC 2163

The eastern side of NGC 2207, the galaxy on the west in Figure 1, lies in front of the ocular galaxy IC 2163. The backlighting by IC 2163 affords a detailed view of the parallel knotty dust streamers in the NGC 2207 arms that cross in front of the central disk of IC 2163. The extinctions in these arms cannot be very large because IC 2163 can still be seen through the disk of NGC 2207. This means that the disk of NGC 2207, aside from the dust streamers, is nearly transparent optically for $R/R_{25} \geq 0.5$ in NGC 2207. Here we adopt $R_{25} = 128''$ from the RC3 and the values of the projection parameters from Paper I. If there are clouds with extremely high extinction, they must occupy only a tiny filling fraction of the disk. The western tidal arm of IC 2163 can be traced in *B* band behind NGC 2207 to within a radius in that galaxy of $R/R_{25} = 0.24$ at position angle 100°. A faint extension might even be visible at $R/R_{25} = 0.17$ and position angle 170° (e.g., see Fig. 3 in Paper III).

The colors of star-forming regions in these galaxies (see § 4.3) also suggest that the average extinction is low. Most of the star-forming regions in IC 2163 lie behind the extended H I envelope of NGC 2207 (see Papers I and III). Nevertheless, the average $B-V$ colors of the star-forming regions on these lines of sight are only 0.26 ± 0.5 mag redder in IC 2163 than in NGC 2207. The $B-V$ color difference is larger in the inner arms of IC 2163, ~0.44 mag redder, but this is still only ~1 mag of extinction.

The surface brightnesses at the locations of dust regions in both galaxies were measured to determine the intrinsic opacities. The positions of these measurements are shown in Figures 3–5. The central region of IC 2163 is in Figure 3, which shows squares for the dust features that appear to reside in NGC 2207, circles for the dust that appears to be in the spiral arms of IC 2163, and crosses for approximate directions of dust measured by Berlind et al. (1997). Measurement positions for the tidal tail of IC 2163 are shown in Figure 4, and the central and western parts of NGC 2207 are shown in Figure 5. We see a lot of small-scale dust structure, with some dust clouds as small as the telescope resolution limit of 0.″1. At each dust position, the measured intensity is an average over a rectangular box that ranges from 2 to 5 pixels on a side, depending on the size of the feature. One pixel equals 0.″1, which is 17 pc, so the dust extinctions are averages inside boxes ranging from 34 to 85 pc on a side. There are likely to be smaller dust clouds inside these measured cells, so the average extinction is weighted by the angular filling factor of the smaller clouds. This is not the same extinction that would be obtained from a uniform medium with the same average column density.

In what follows, various methods for quantifying the extinction in NGC 2207 and IC 2163 are discussed: § 3.1 employs the method of White & Keel (1992) and Berlind et

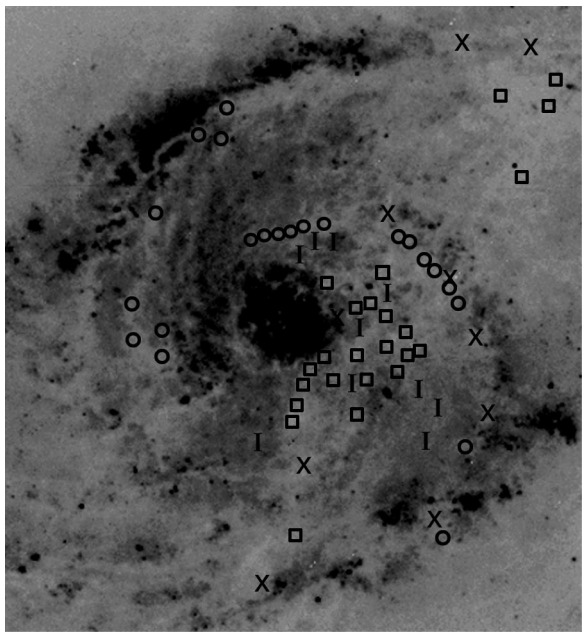

FIG. 3.—*I*-band image of the central region of IC 2163, showing measured dust clumps in the streamers of NGC 2207 across the face of IC 2163 (*squares*), dust regions previously measured on ground-based images by Berlind et al. (*crosses*), dust regions along the western inner spiral and eyelid regions of IC 2163 (*circles*), and intercloud regions (*I*).

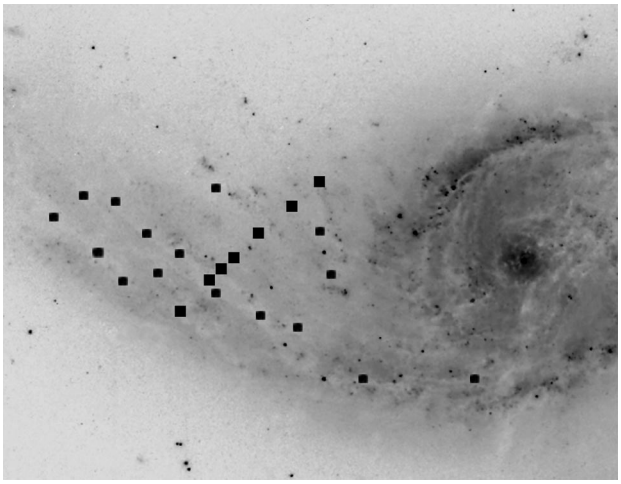

FIG. 4.—V-band image of the eastern half of IC 2163, showing measured dust regions in the tidal arms (*squares*).

al. (1997) for the opacity in the parts of these galaxies that overlap on the line of sight. Section 3.2 derives the excess extinction in these and other dust features using local magnitude differences and radiative transfer models.

3.1. *Dust Extinction in NGC 2207 from the White & Keel Method*

White & Keel (1992) measured the extinction through a foreground galaxy using another galaxy as a background source. If $I_{\rm bkg}$ is the background intensity that would be measured in the absence of the foreground galaxy, $I_{\rm fore}$ is the intensity that would be measured in the foreground galaxy in the absence of the background galaxy, and τ is the extinction in the foreground galaxy, then the observed total intensity at an overlap position is $I_{\rm fore} + I_{\rm bkg}e^{-\tau}$. The opacity of the foreground dust can be estimated from this equation if the total intensity at the position of the dust cloud is measured and the foreground and background intensities of the two galaxies are estimated from the nonoverlapping points in each galaxy that are located diametrically opposite the dust position of interest. This method assumes that the galaxy comparison intensities are the same as those at the dust region.

Berlind et al. (1997) applied the White & Keel (1992) method to the overlapping regions of IC 2163 and NGC 2207 by using ground-based optical and near-IR photometry. Their measurements suggested that the J-band extinction in a main spiral arm is higher by a factor of ~ 1.3 compared with the B, V, and R extinctions than that expected from the Whitford reddening curve (see Rieke & Lebofsky 1985 for the Whitford curve), and they interpreted this result as evidence for either a different reddening law or unresolved patchy dust (which is better resolved on our *HST* images).

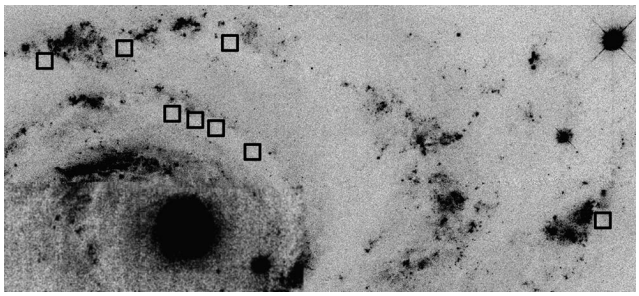

FIG. 5.—B-band image showing the locations of the dust features measured (*squares*) in the western half of NGC 2207.

We tried the method of White & Keel on the *HST* data but had several difficulties. First, there are large variations in intensity and star formation rate throughout the disks of both galaxies, making the comparison intensities and colors uncertain. A high estimate for the background intensity and too red a background intensity make a Whitford reddening law in the overlap region appear gray. Second, H I from NGC 2207 lies in front of the comparison region of IC 2163, providing foreground dust, but the gas there is probably as patchy as the dust we see elsewhere. This means a precise reddening correction for the background points cannot be determined. The resulting cloud opacities measured with the White & Keel method from the *HST* data are therefore uncertain, as is the reddening law. For example, the extinctions we measure yield a scatter of a factor of ~ 2 in A_λ/A_V for U and B passbands.

The White & Keel method can be illustrated anyway using the B, V, and I passbands, which had the smallest noise for each measurement and the smallest point-to-point fluctuations in the background. To determine the intensities in the comparison regions for IC 2163, I_{2163}, we transformed the sky-view images to polar coordinates, (r, θ), for distance from the center, r, and azimuthal angle, θ, measured counterclockwise from north. The background intensity from IC 2163 was assumed to be the same as the intensity in a comparison region on the eastern side of IC 2163 at the approximate radius of the dust feature and an azimuthal angle between 25° and 65°. The comparison regions were chosen to be free of discernible dust filaments and obvious star-forming regions, but they still contain dust and slight foreground emission from NGC 2207. We estimate the 1 σ standard deviation in sky-subtracted IC 2163 surface brightness from pixel noise and point-to-point fluctuations to be ± 0.7, ± 0.3, ± 0.1, and ± 0.08 mag in U, B, V, and I, respectively. These errors are given by $2.5 \log [(C + N)/C]$ for average number of counts, C, and total rms noise in the counts, N.

The comparison intensity for NGC 2207, I_{2207}, depended on whether we were measuring the arm or the interarm dust. For the arm dust, we used dust lanes in the same spiral arm in the northern part of NGC 2207, which does not overlap IC 2163. This gives only an approximation because this part of the spiral arm is at a smaller radius than the dust features. For the interarm dust, we used interarm regions of NGC 2207 that were diametrically opposite. The rms deviations of the sky-subtracted surface brightnesses for the foreground emission from NGC 2207 in the case of the spiral arm dust regions were ± 1.6, ± 0.9, ± 0.8, and ± 0.6 mag in U, B, V, and I, respectively. For the interarm dust regions, they were ± 2.4, ± 1.1, ± 0.9, and ± 0.6 mag, respectively.

The extinction from the part of NGC 2207 that covers IC 2163 in the comparison region was estimated from the H I map. Foreground H I is clearly separate in velocity from the H I in IC 2163, so the average column density of gas in front of the comparison region can be determined. Because the comparison region of IC 2163 is overlapped by the outer part of NGC 2207, which is likely to be metal-poor, we take $A_V = (0.35 \pm 0.18) \times 10^{-21} N(\text{H I})$ for a metallicity

of $\frac{2}{3}$ the solar value (see Bohlin, Savage, & Drake 1978). We selected comparison regions in IC 2163 where the foreground H I column density due to NGC 2207 is relatively low, $\sim 10^{21}$ atoms cm^{-2} as measured in the H I map with resolution $13''.5 \times 12''$. We adopted a constant correction for extinctions in front of the eastern side of IC 2163 equal to 0.54, 0.46, 0.35, and 0.15 mag in U, B, V, and I bands, respectively, for a Whitford reddening curve. These extinctions are probably accurate only to a factor of 2 because of point-to-point variations.

The results of the extinction measurements are presented in Table 1 along with the estimated errors and point-to-point variations. Corrected for the foreground H I, the average B-, V-, and I-band extinctions in 24 foreground clouds in the overlap region of NGC 2207 are 2.3 ± 0.8, 1.5 ± 0.4, and 0.9 ± 0.3 mag in B, V, and I bands, respectively. These standard deviations are from point-to-point variations and are listed in Table 1 as "variations." Additional errors come from pixel noise in the sky and cloud measurements and from point-to-point variations in the sky. These additional errors are listed in Table 1 as "errors." The pixel and sky errors are independent of the point-to-point variations in the cloud measurements and can be smaller. The average extinctions in 10 intercloud regions are 1.2 ± 0.7, 1.0 ± 0.5, and 0.7 ± 0.3 for B, V, and I, respectively. For the five "spiral arm" directions studied by Berlind et al. (these are the cloud points shown in Fig. 3), the average extinctions are 2.2 ± 0.4, 1.7 ± 0.4, and 1.2 ± 0.6, respectively, in these three passbands, and for the five "interarm" positions studied by Berlind et al. (these are intercloud regions listed in Table 1), they are 1.5 ± 0.9, 1.2 ± 0.5, and 1.1 ± 0.6 mag, respectively. In most cases, the total measurement error for A_V and A_I is somewhat less than the standard deviation quoted here.

For comparison, the average extinctions derived by Berlind et al. but corrected for the foreground H I are 1.9 ± 0.1 and 1.4 ± 0.1 mag in B and V, respectively, for the spiral arm regions and 1.1 ± 0.1 and 0.9 ± 0.1 mag in B and V, respectively, for the interarm. Our *HST* values at these positions are consistent with the corrected Berlind et al. values within the standard deviations of the means.

3.2. *Radiative Transfer Models of Extinction in NGC 2207 and IC 2163 Based on Magnitude Differences in Dust Regions*

The White & Keel method works best when the foreground and background galaxies are symmetric and smooth. Then the comparison regions accurately represent the unseen intensities that are needed to determine the opacity in a foreground cloud. At the high resolution of the *HST* observations, however, small-scale variations in the dust and star formation make it unlikely that good comparison regions can be found in these galaxies. As a result, the extinctions measured in the previous section are imprecise.

To get around this problem, we measured the magnitude differences between dust features and the immediately adjacent regions in the same galaxy, and we fitted radiative transfer models to these measurements to derive the corresponding extinction differences. This method does not require intensities from diametrically opposite parts of the galaxy. Figure 3 shows the regions used for this method as circles and squares, while Figures 4 and 5 show the regions as squares.

The radiative transfer analysis uses the intensities from three *HST* passbands, B, V, and I. The stellar disks are assumed to have the same vertical stratification of emission measure as in the local Milky Way, considering that we have no detailed information about this for another galaxy. This yields relative dimensionless midplane emissivities of 9.8, 8.6, and 11.4 in B, V, and I, and scale heights for Gaussian distributions around the midplane of 92, 110, and 164 pc, respectively (from Elmegreen 1980). The reddening curve is assumed to follow a Whitford extinction law, with 1 mag extinction in visible band corresponding to a gaseous column density of 1.87×10^{21} cm^{-2} (Bohlin et al. 1978). The vertical dust distributions are assumed to be Gaussian, with the same scale height for the cloud and intercloud regions in each galaxy.

For dust regions in NGC 2207 that are foreground to IC 2163, or for those in IC 2163 that are background to NGC 2207, we also need the ratio of the volume emissivity in IC 2163 to the volume emissivity in NGC 2207, and we need to make assumptions about the relative brightnesses of the foreground and background regions. Here we assume for the foreground dust clouds that the background emission comes from an intercloud region in IC 2163; we also assume for the background dust clouds that the foreground emission is from an intercloud region. These assumptions leave four fitting parameters for the model in the case of the overlap regions: the cloud and intercloud extinctions in NGC 2207 and IC 2163 (and we assume that these intercloud extinctions are the same), the gaseous scale height relative to the stellar scale height, and the relative emissivity

TABLE 1

EXTINCTIONS BY THE METHOD OF WHITE & KEEL

Foreground Region and Location	A_B	A_V	A_I
Average, 24 clouds	2.3	1.5	0.9
Variations, 0.62–0.69 R/R_{25}	± 0.8	± 0.4	± 0.3
Errors	± 1.3	± 0.3	± 0.2
Average, 5 clouds at Berlind pts.	2.2	1.7	1.2
Variations, 0.63–0.80 R/R_{25}	± 0.4	± 0.4	± 0.6
Errors	± 1.3	± 0.3	± 0.2
Average, 10 intercloud regions	1.2	1.0	0.7
Variations, 0.59–0.80 R/R_{25}	± 0.7	± 0.5	± 0.3
Errors	± 0.7	± 0.2	± 0.2
Average, 5 intercloud regions at Berlind pts.	1.5	1.2	1.1
Variations, 0.63–0.80R/R_{25}	± 0.9	± 0.5	± 0.6
Errors	± 0.7	± 0.2	± 0.2

of IC 2163 compared with NGC 2207. For nonoverlapping regions, we need the cloud and intercloud extinctions and the relative scale heights of the dust and stars; we do not need the ratio of emissivities of the two galaxies.

Figure 6 in the bottom panel shows model results for the relative extinction between cloud and intercloud regions in NGC 2207 that occurs in the overlapping regions. The top panel shows the observations at the locations indicated in Figure 3 (*squares only*). The solid lines for the models have a line-of-sight component of the gaseous scale height equal to 100 pc, which corresponds to a deprojected scale height $H_{\rm gas} = 77$ pc for an inclination of 40°; this is slightly smaller than the blue light scale height given above. The solid lines also have a galaxy volume emissivity ratio j(IC2163)/j(NGC2207) = 10 in all passbands, a midplane intercloud density of 1 cm^{-3} (giving a total intercloud extinction of 0.25 mag in V perpendicular to the disk), and midplane densities in the dust cloud of 2, 3, 4, and 5 cm^{-3}. The value adopted for the galaxy volume emissivity ratio is motivated by the value of the surface brightness ratio I_{2163}/I_{2207} from the modified White & Keel method in § 3.1. The dashed lines have the same j(IC2163)/j(NGC2207) = 10, but a deprojected scale height that is twice as large, $H_{\rm gas} = 150$ pc, a midplane intercloud density that is half as much, 0.5 cm^{-3}, and midplane cloud densities 1, 1.5, 2, and 2.5 cm^{-3}. This larger gaseous scale height might be reasonable because of the large velocity dispersion of the H I gas (see Paper I). The dot-dashed lines have j(IC2163)/j(NGC2207) = 1 with $H_{\rm gas} = 150$ pc, a midplane intercloud density of 0.5 cm^{-3}, and midplane densities in the dust cloud of 1, 1.5, 2, 2.5, 3, and 3.5 cm^{-3}. The dotted lines have a larger intercloud extinction: the scale height is $H_{\rm gas} = 150$ pc, the midplane intercloud density is 1 cm^{-3}, the emissivity ratio is j(IC2163)/j(NGC2207) = 10, and the dust cloud densities are 1.5, 2, 2.5, and 3 cm^{-3}.

All of these models yield magnitude differences that are in the observed range for NGC 2207 features. The intrinsic extinction of a modeled region comes from the product of the midplane density and twice the scale height divided by the extinction-to-gas conversion ratio. For the solid line, the intercloud extinction is ~0.5 mag and the dust extinctions in the figure range from 1 to 2.5 mag. These results are comparable to what we found using the method of White & Keel.

Figure 7 at the top shows the magnitude differences for dust features in the tidal tail of IC 2163 (Fig. 4) and for the nonoverlapping regions of NGC 2207 (*dashed lines*). A dark cloud in the western spiral arm of NGC 2207 is not included (see below). At the bottom, this figure shows the appropriate models for radiative transfer in a single galaxy. The line types at the bottom are the same as in the previous figure; solid lines are for a deprojected gaseous scale height $H_{\rm gas} = 100 \cos i = 77$ pc, a midplane intercloud density of 1 cm^{-3}, and midplane densities in the dust cloud of 2, 3, 4, 5, and 6 cm^{-3}. The dashed lines have $H_{\rm gas} = 200 \cos i = 150$ pc, a midplane intercloud density of 0.5 cm^{-3}, and midplane cloud densities of 1, 1.5, 2, 2.5 and 3 cm^{-3}. The dotted lines

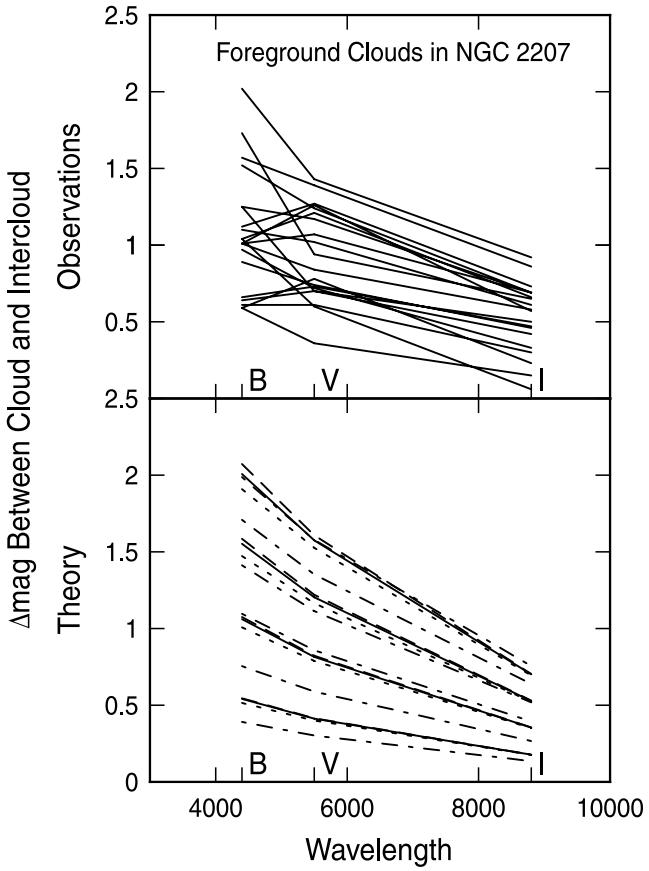

FIG. 6.—*Top*, Observations of the magnitude differences between dust features and the surrounding regions for clouds that appear to reside in NGC 2207 in the regions that are foreground to IC 2163 (Fig. 3, *squares*); *bottom*, models of such foreground clouds. The solid lines represent models with a deprojected gaseous scale height of $H_{\rm gas} = 77$ pc, a ratio of volume emissivities of IC 2163 compared with NGC 2207 equal to 10, a midplane intercloud density of 1 cm^{-3}, and midplane cloud densities of 2, 3, 4, and 5 cm^{-3}. For the dashed lines $H_{\rm gas} = 150$ pc, the emissivity ratio is 10, intercloud density is 0.5 cm^{-3}, and cloud densities are 1, 1.5, 2, and 2.5 cm^{-3}. For the dot-dashed lines $H_{\rm gas} = 150$ pc, the emissivity ratio 1, intercloud density is 0.5 cm^{-3}, and dust cloud densities are 1, 1.5, 2, 2.5, 3, and 3.5 cm^{-3}. For the dotted lines $H_{\rm gas} = 150$ pc, the emissivity ratio is 10, intercloud density is 1 cm^{-3}, and cloud densities are 1.5, 2, 2.5, and 3 cm^{-3}.

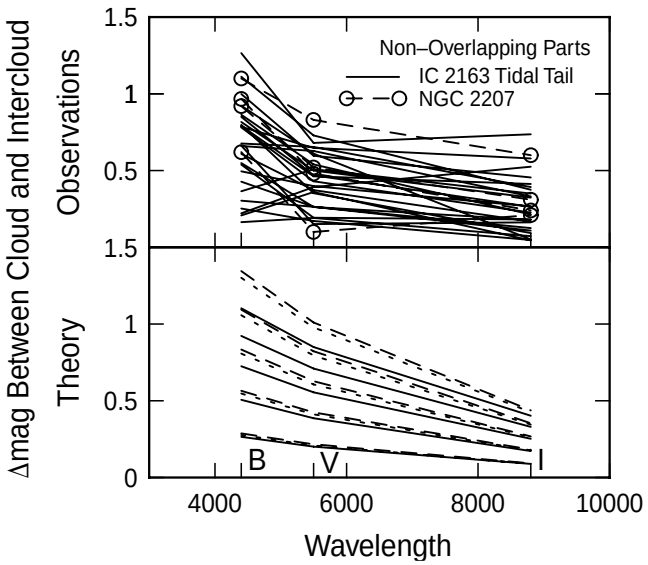

FIG. 7.—*Top*: Observations of the magnitude differences between dust features and the surrounding regions for clouds that reside in the tidal tail of IC 2163 (see Fig. 4) and in the nonoverlapping regions of NGC 2207 (*dashed lines*; see Fig. 5). The dark cloud in the western spiral arm of NGC 2207 is not included. *Bottom*: Models of such nonoverlapping clouds. The line types are the same as in Fig. 6, except that the ratio of volume emissivities for the two galaxies does not matter here.

have a scale height $H_{gas} = 150$ pc, midplane intercloud density 1 cm^{-3}, and dust cloud densities 1.5, 2, 2.5, and 3, and 3.5 cm^{-3}.

The absence of an azimuthal gradient in excess extinction between the northern dust filaments on the tidal tail and those near its southern edge is consistent with the interpretation in Paper III that these filaments are stretched flocculent spiral arms that were present before the interaction.

Figure 8 compares observations and theory for the background dust clouds of IC 2163 that are in the overlap region (see Fig. 3). The line types are the same as in Figure 6, including the same ratios of volume emissivities for the two galaxies. The midplane densities are the same also for each line type, but the lowest density in Figure 7 is not plotted in Figure 8. The case with j(IC2163)/j(NGC2207) = 1 yields magnitude differences that are too low for this case. In these models, the background dust cloud is assumed to have a foreground distribution of stars and dust from NGC 2207 that corresponds to an intercloud region in NGC 2207. Uniform foreground starlight decreases all the magnitude differences even if the intrinsic cloud extinctions are the same. The models fit the data adequately.

Regardless of whether the clouds are in the foreground part of NGC 2207, the background part of IC 2163, or in the nonoverlapping regions, the model predicts the observed range of magnitude differences. The results suggest that the range of intrinsic cloud opacities is about the same in all regions of the two galaxies. The apparent magnitude differences vary from region to region, depending on the presence of uniform foreground emission or absorption, but the cloud properties do not vary much. The intercloud extinction, measured perpendicularly through the disk, ranges from 0.25 to 0.5 mag in V, and the cloud extinctions range from 0.5 to 1.7 mag in the various models. The line-of-sight extinctions are larger by 1.3 because of the inclination, i.e., the averages become 0.5 and 1.4 mag in the intercloud and cloud regions, respectively. These results are slightly smaller than the line-of-sight intercloud and cloud extinctions obtained by the White & Keel method for the overlap regions, which on average are ~1.1 and ~1.6 mag, respectively, in V (the average is taken over our 24 cloud points and the five Berlind et al. cloud directions, and over our 10 intercloud points and the five Berlind et al. intercloud directions; see § 3.1). The difference between the extinctions obtained by the radiative transfer method and the White & Keel method is most likely the result of uncertain assumptions and large inaccuracies for each.

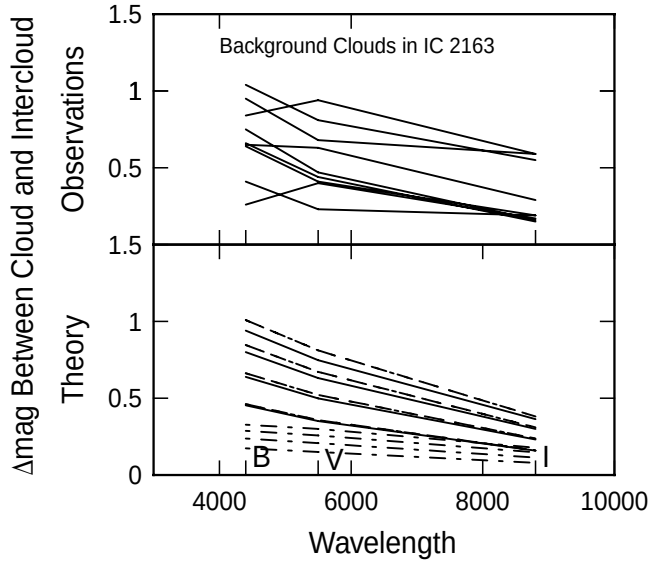

FIG. 8.—*Top*, observations of the magnitude differences between dust features and the surrounding regions for clouds of IC 2163 that are in the overlap region behind NGC 2207 (Fig. 3, *circles*); *bottom*, models of such background clouds. The line types are the same as in Fig. 6.

An exception to this uniformity of cloud properties occurs for the dark conical cloud that lies near the bright star-forming region and radio continuum source in the westernmost arm of NGC 2207 (discussed in Paper III). This cloud appears to be unusually dense and thick. Its magnitude differences are all large, and they are nearly equal for all passbands: $\Delta m_U = 1.78$, $\Delta m_B = 1.73$, $\Delta m_V = 1.24$, and $\Delta m_I = 1.38$. The true extinction to the center of this cloud could be several tens of magnitudes, and the bulk of it could lie in the foreground, on the near side of the midplane of NGC 2207. Considering its conical shape and the bright analogous cone of emission that extends away from the central cluster in the other direction (Paper III), it could be the near side of a 500 pc–long chimney.

The lack of similarly dark clouds elsewhere in these galaxies does not mean they are not present; it means only that the darkest molecular clouds are either too small to be seen or that they are surrounded by bright intensity from reflection nebulae or ionized gas.

4. STAR-FORMING REGIONS IN IC 2163 AND NGC 2207

4.1. *Method of Analysis*

Star-forming regions were measured in IC 2163 and NGC 2207 from the limit of resolution of 1 WF pixel = 16.8 pc diameter or 1 PC pixel = 7.7 pc diameter, to extended star formation sites with diameters of 800 pc. A total of 103 regions were measured in IC 2163 and 184 regions in NGC 2207, selected to have a signal-to-noise ratio greater than 3 to reduce uncertainties in the colors.

The instrumental magnitudes were converted to Johnson magnitudes using the relations given in the WFPC2 photometry handbook, assuming the conversions for early-type stars: $U = U_{HST} + 0.46$, $B = B_{HST} + 0.66$, $V = V_{HST} + 0.05$, $I = I_{HST} - 1.13$. These conversions are accurate to approximately 0.05 mag. The background intensity underlying the star-forming regions was subtracted by measuring several regions adjacent to each star formation site and averaging over their intensities. For example, if the star-forming region was in a spiral arm, then the arm background was measured for subtraction; if it was in an interarm region, the interarm was subtracted. These measurements were made from intensity cuts through the regions, as well as photometry measurements surrounding the regions. Because of variable extinction and the exponential galaxy background, the background intensity measurement had the greatest uncertainty. An estimated uncertainty of ~10% in the backgrounds leads to errors of 0.14 in V magnitude and 0.20 in $V-I$ color, although some regions (described below) may require corrections as high as 0.4 mag. For each measurement, a foreground Milky Way extinction correction was subtracted from the calibrated magnitude by using $A_B = 0.49$ mag (from Burstein & Heiles 1982, using H I maps) for B band. Assuming a Whitford law, these corrections were $A_U = 0.57$, $A_V = 0.37$, and $A_I = 0.16$ mag in U, V, and I bands, respectively. More recent results

posted on NED (from Schlegel et al. 1998 using IRAS and DIRBE) yield $A_B = 0.374$ mag; with this correction, our objects would be 0.09 mag fainter in V and 0.03 mag redder in $B-V$ than with the Burstein & Heiles values.

4.2. *Size-Luminosity Relation and Fractal Dimension*

The size-luminosity relation for the star-forming regions in each galaxy is shown in Figure 9, where M_V is plotted versus the logarithm of the diameter. The different symbols correspond to different radial positions, from the inner spiral to the eyelid region to the outer spiral in IC 2163, and from the inner to the outer spiral in NGC 2207. The largest and brightest star-forming regions in both galaxies are in the outer parts.

The magnitudes of the star-forming regions, aside from the super–star clusters (SSCs; see § 4.4), increase with the logarithm of the diameters approximately as $M_V \approx (0.5 \pm 0.4) - (5.4 \pm 0.4)\log D$ for NGC 2207 and $M_V \approx (-1.1 \pm 2.5) - (4.1 \pm 0.6)\log D$ for IC2163, which convert to a relation between luminosity, L, and diameter: $L \propto D^{2.17 \pm 0.15}$ for NGC 2207 and $L \propto D^{1.63 \pm 0.13}$ for IC 2163. These results come from bivariate fits to the points in Figure 9 and are similar to the result Elmegreen & Salzer (1999) obtained for star-forming complexes in a sample of 11 intermediate and late-type spiral galaxies. The correlation suggests that the complexes have similar surface brightnesses.

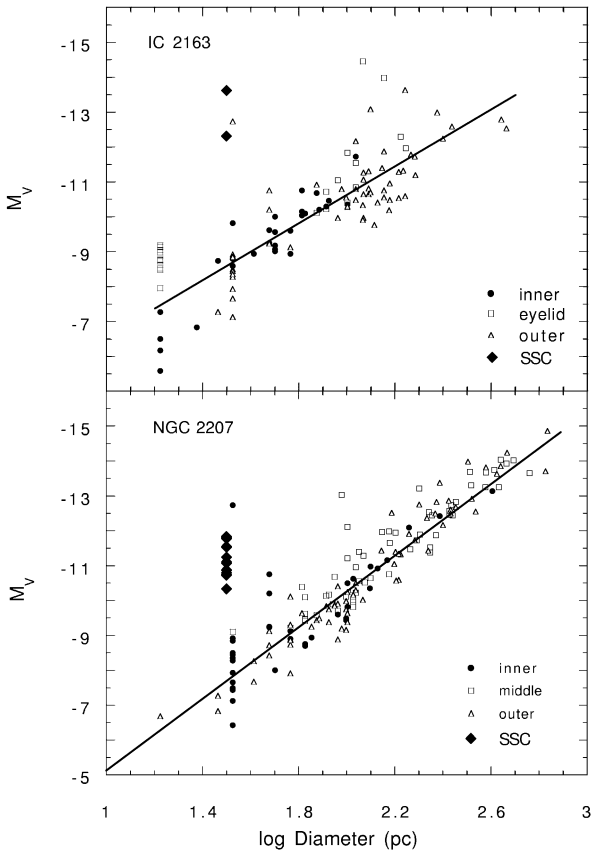

FIG. 9.—Absolute V magnitude versus diameter (in parsecs) for the measured star-forming regions in both galaxies, coded according to their locations in the galaxies. The lines show bivariate least-square fits. Diamonds indicate super–star clusters, which are abnormally bright for their size compared with normal star-forming regions.

The power in the luminosity-diameter relation can be identified with the fractal dimension (Mandelbrot 1983). It is not accurately determined here, but it appears to be consistent with the fractal dimension of interstellar clouds in the Milky Way and other galaxies (Gill & Henriksen 1990; Larson 1992; Pfenniger & Combes 1994; Elmegreen & Falgarone 1996; Heithausen et al. 1998; Westpfahl et al. 1999; Keel & White 1999). If this is the case, then the star-forming regions in NGC 2207 and IC 2163 have the same geometric structure as typical interstellar gas (for a review of this point, see Elmegreen et al. 2000a, 179).

4.3. *Color-Magnitude and Color-Color Diagrams*

Color-magnitude diagrams with M_V versus $V-I$ for the measured star-forming regions are shown in Figure 10 for IC 2163 and NGC 2207. The range of brightness and color of the normal star-forming regions is the same in each galaxy, although overall the star-forming regions are slightly less luminous in IC 2163. The ocular (eyelid) structure of IC 2163 and the inner arms of NGC 2207 are highlighted by strings of young clusters, and the northern arm of NGC 2207 has several super–star clusters. Most of the star-forming regions occur in Hα-emitting regions, although the poor resolution of the ground-based Hα image precludes a direct comparison.

Most of the regions in IC 2163 are obscured by NGC 2207. Some of the star-forming regions at the extreme color limits suffer from uncertain background subtraction due to dust variations and cannot be measured to better than 0.4 mag; 11% of the regions in IC 2163 and 10% of the regions in NGC 2207 are in this category. Correcting for dust extinction as in § 3 shifts the $V-I$ colors bluer than those shown in the figure by 0.23 mag on average and their absolute V magnitudes by about 0.36 mag brighter. The reddest region on the IC 2163 plot in Figure 10, at $V-I = 2.3$, is in a dust lane of NGC 2207 and shifts bluer by 0.4 mag after dust correction.

To estimate the ages and masses of star-forming regions, starburst models by Leitherer et al. (1999, hereafter Starburst 99) are also shown for M_V versus $V-I$ in Figure 10 for instantaneous star formation with a Salpeter mass function. There is no substantial difference between the models for high and low metallicity, so only the $z = 0.04$ models are shown here. Evolution lines are drawn for cluster masses of 10^5 and $10^6\ M_\odot$. Ages along the model lines are indicated by crosses placed in $\Delta \log t = 0.5$ intervals, where t is in years, from 10^6 yr on the upper left to 10^9 yr at the bottom of the model line. The $V-I$ model colors range from ~ -0.3 to ~ 1.5 between the ages of 10^6 and 10^9 yr, with the reddest color corresponding to ages of $\sim 8 \times 10^6$ yr.

The majority of the star-forming regions in both galaxies have $V-I$ colors between -0.2 and 0.6 mag, which corresponds to ages less than or equal to 6×10^6 yr. The model results are double-valued at $V-I > 0.6$ mag, which corresponds to ages that are either between 6×10^6 and 8×10^6 yr or between 8×10^6 and 10^8 yr. The locations of the star-forming regions in the $B-V$ versus $V-I$ color-color diagram are consistent with ages less than 6 Myr for almost all the star-forming regions. For the inferred ages, the star-forming regions have masses ranging from 10^3 to $10^6\ M_\odot$.

Color-color diagrams of clusters are shown in Figure 11 for the star-forming regions in both galaxies. The line represents a correction of 1 mag of visual extinction. The average $V-I$ is about the same for both galaxies,

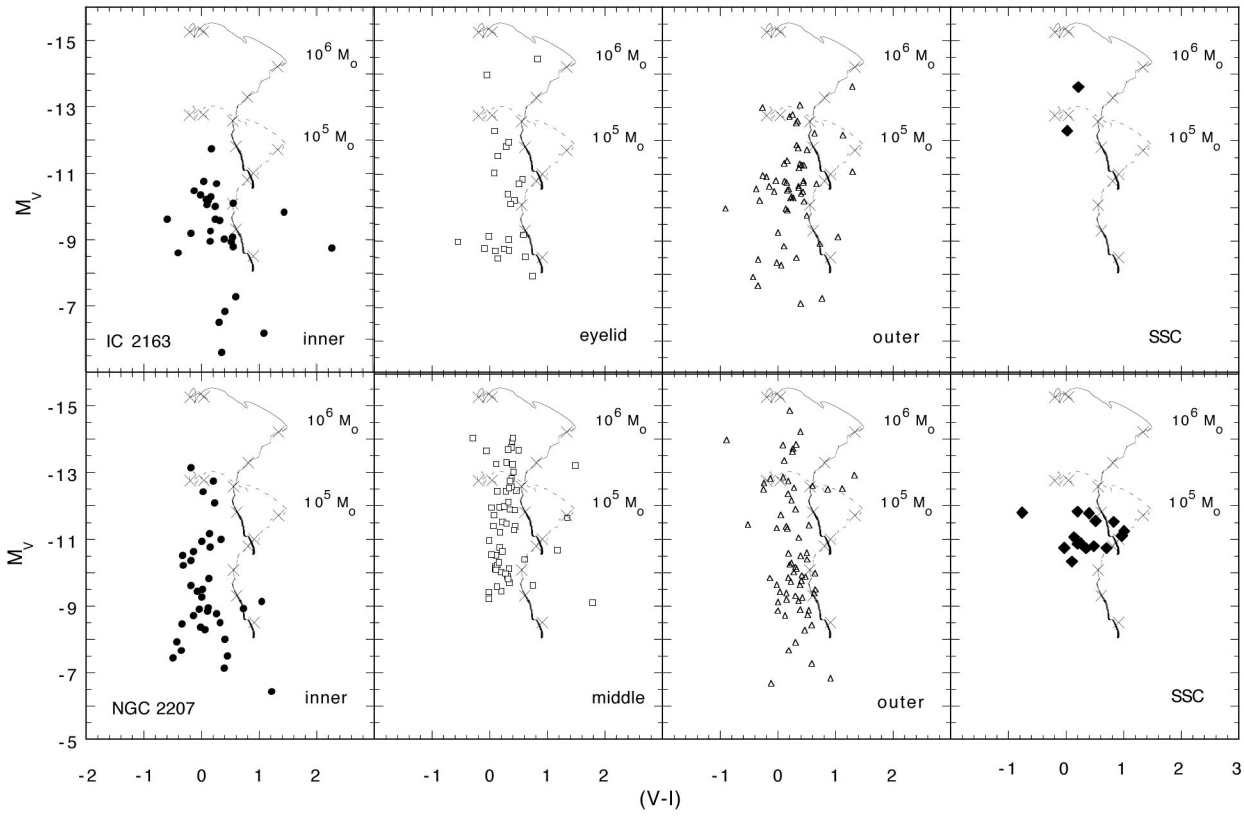

FIG. 10.—Color-magnitude diagrams for star-forming regions in IC 2163 and NGC 2207, with the same coding as in Fig. 6. The upper panels show inner, eyelid, outer, and SSC regions in IC 2163, and the lower panels show inner, middle, outer, and SSC regions in NGC 2207. Starburst 99 instantaneous models with a Salpeter mass function and metallicity $z = 0.04$ (Starburst 1999) are also shown as solid lines for clusters with mass 10^6 and 10^5 $M_\odot$. Crosses on the lines denote time intervals of log $t = 0.5$, where t is in years, starting with log $t = 6$ on the upper left of each line and continuing to log $t = 9$ at the lower end. Most star-forming regions have ages of a few times 10^6 yr; their masses range from several times 10^3 to several times 10^5 $M_\odot$.

0.27 ± 0.40 mag for NGC 2207 and 0.28 ± 0.42 mag for IC 2163. The average $B-V$ is nearly 0.3 mag bluer for NGC 2207 than for IC 2163: -0.13 ± 0.38 mag compared with 0.13 ± 0.41 mag, respectively. Within the errors these are not significant differences, but it is reasonable for the regions in IC 2163 to be redder because of their obscuration by NGC 2207. The excess visual extinction of ~ 1 mag found in § 3 corresponds to a $B-V$ value that is redder by 0.3 mag, as observed.

4.4. *Super–Star Clusters*

Two regions in IC 2163 and 15 in NGC 2207 have star-like intensity profiles that are well fitted by Gaussians. They have average absolute visual magnitudes of approximately -13 in IC 2163 and approximately -11 in NGC 2207. These regions could be super–star clusters like those observed in other interacting galaxies. They are indicated in Figures 9–11 by diamonds, and their locations are outlined by squares in enlarged images in Figure 12. Most of the SSCs occur in Hα-emitting regions. Two of the SSCs (numbered 13 and 14) are in the region of the strong radio continuum source in the far western part of NGC 2207 (see Paper III). The recent supernova SN 1999ec occurred 1.″7 east and 3.″3 south of SSC 14.

SSCs observed in other galaxies are inferred to have diameters of 8–10 pc (e.g., Watson et al. 1996), which is smaller than the resolution of our images. The Gaussian fits to the SSCs in IC 2163 and NGC 2207 yield an FWHM ranging from 1.19 to 3.05 pixels, which corresponds to 20–50 pc, considering that 1 pixel = 17 pc. If we subtract in quadrature the FWHM of a stellar image, which is ~ 1.8 pixels, then the SSC FWHMs extend from near-zero size up to ~ 40 pc; these corrected diameters are used in Figure 9. The largest clusters are bigger than SSCs in other galaxies.

SSCs were also observed in the merger remnant galaxy NGC 7252 (Miller et al. 1997), which is nearly twice as far away as IC 2163 and NGC 2207. Miller et al. estimated sizes for their clusters that are smaller than their resolution limit, based on photometry through different apertures. We compared the magnitudes of our SSCs measured with 2 and 5 pixel radius apertures, which was the method Miller et al. used to discriminate between diffuse and centrally peaked regions. Restricting our photometry to a 2 pixel radius aperture for these regions, we measured visual absolute magnitudes of -10 to -13.5, with $V-I$ colors ranging from -0.2 to 1. With a 5 pixel aperture, the magnitudes range from -10.3 to -13.7 with similar colors. We conclude from the similarity of the measurements in the two apertures that these are centrally peaked sources. The 5 pixel measurements are shown in the figures and the values are listed in Table 2, which provides a summary of our SSC data.

Besides NGC 7252, SSCs are also seen in the interacting galaxies NGC 4038/4039 (the Antennae; Whitmore et al. 1999) and starburst galaxies such as NGC 253 (Watson et al. 1996). For ease in comparing our data with that of others, we show color-magnitude and color-color diagrams in Figures 13 and 14, respectively. Three different ages of

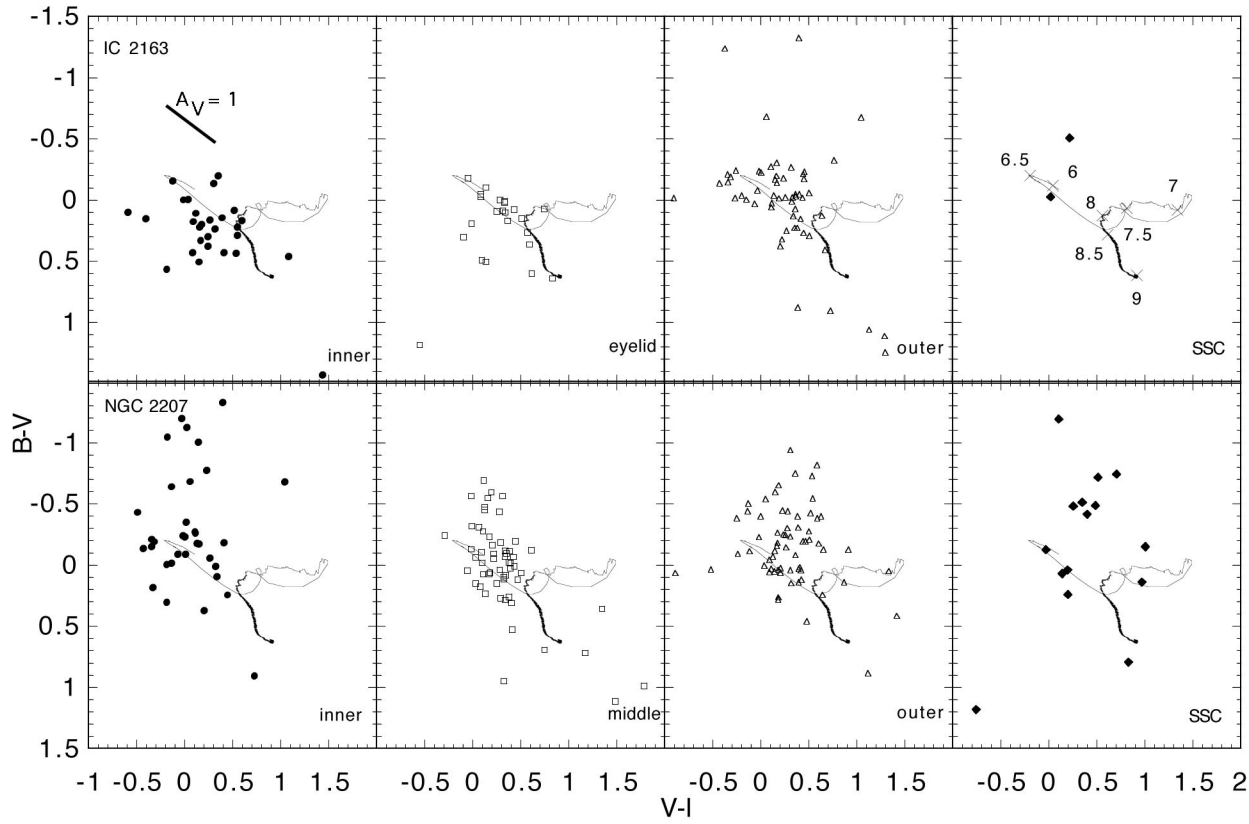

FIG. 11.—Color-color diagrams for the star-forming regions in both galaxies, separated by regions as in Fig. 10. The lines show colors for Starburst 99 instantaneous models as a function of time, indicated by tick marks in intervals of log $t = 0.5$, where t is in years, in the right-hand panels. The numbers indicate log t in the upper right panel. A correction for 1 mag of visual extinction would be shifted as indicated by the line in the upper left panel. As in Fig. 10, most regions have ages of a few times 10^6 yr, although some regions are too blue in $B-V$ to be well fitted by the models.

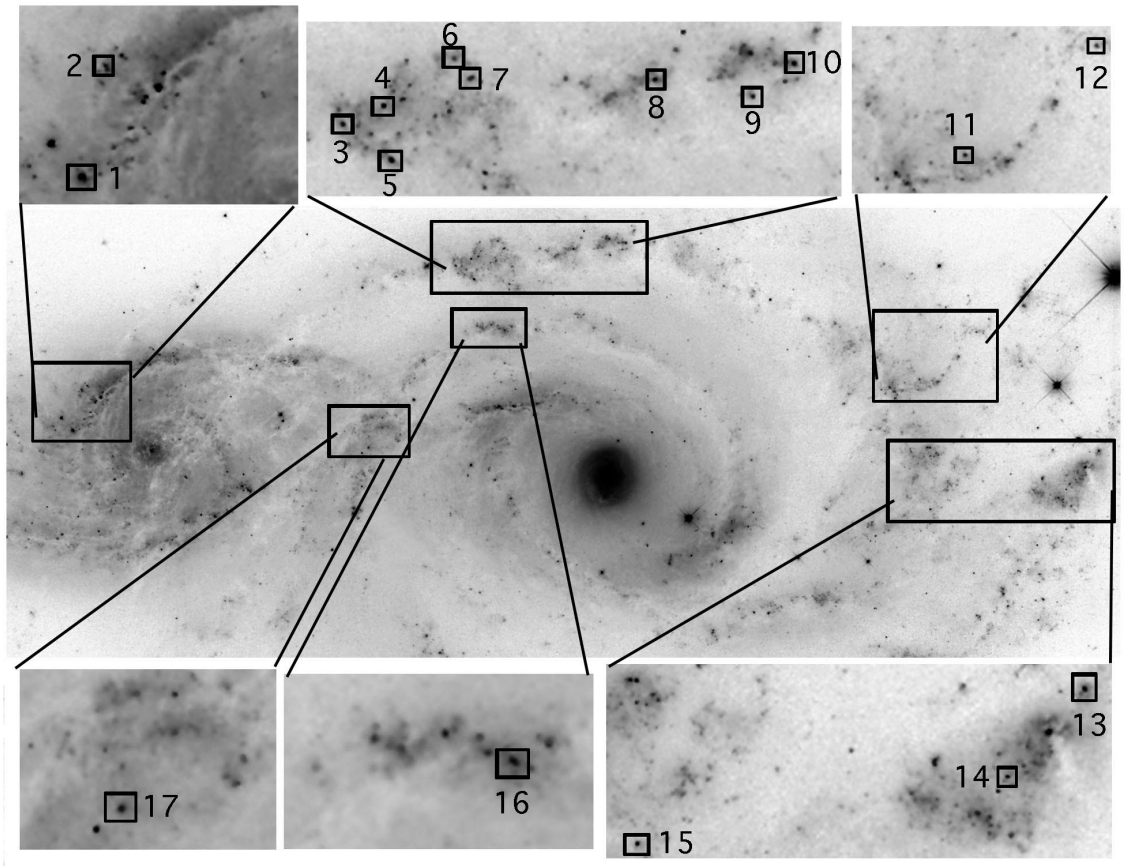

FIG. 12.—Candidate SSCs (*squares*) and their locations (*rectangles*) in IC 2163 and NGC 2207 on the mosaic image

TABLE 2

SUPER–STAR CLUSTERS

SSC	M_V	$U-B$	$B-V$	$V-I$	Mass ($10^4\ M_\odot$)
1.....	−13.6	−2.5	−0.5	0.2	20
2.....	−12.3	−1.7	−0.0	0.0	6.0
3.....	−10.7	−1.9	−0.5	0.3	2.0
4.....	−11.1	−1.1	0.1	1.0	2.7
5.....	−11.5	−2.9	0.8	0.8	2.7
6.....	−10.8	−1.8	−0.5	0.5	2.0
7.....	−11.1	−1.9	0.1	0.1	2.0
8.....	−11.2	−1.6	−0.1	1.0	2.7
9.....	−10.9	−2.0	−0.5	0.3	2.0
10.....	−11.8	−1.4	1.2	−0.8	2.5
11.....	−10.7	−1.9	−0.4	−0.0	1.5
12.....	−10.3	−1.2	−1.2	0.1	1.0
13.....	−11.8	−1.9	−0.4	0.4	2.7
14.....	−10.7	−1.1	−0.7	0.7	2.1
15.....	−10.9	−2.1	0.0	0.2	2.0
16.....	−11.5	−1.6	−0.7	0.5	2.7
17.....	−11.8	−1.9	0.2	0.2	2.7

Antennae SSCs are shown, along with the SSCs in NGC 7252 and in our galaxies, all transformed to the Johnson system. Our SSCs are about 1 mag fainter in V than the young Antennae SSCs and about the same as the majority of the NGC 7252 SSCs. The $V-I$ range is similar for our SSCs, the young Antennae, and some NGC 7252 SSCs, although our SSCs are bluer in $B-V$ by about 0.5 mag on average. Our SSCs occupy the same part of the $B-V$ versus $V-I$ diagram as a significant number of our well-resolved star-forming regions shown in Figure 11.

The colors and magnitudes of the SSCs allow us to determine their ages and masses. Most have ages of a few times 10^6 yr. Some colors are in the double-valued region of Figure 13, so the corresponding ages could either be between $\sim 6 \times 10^6$ and 8×10^6 yr or between 8×10^6 and

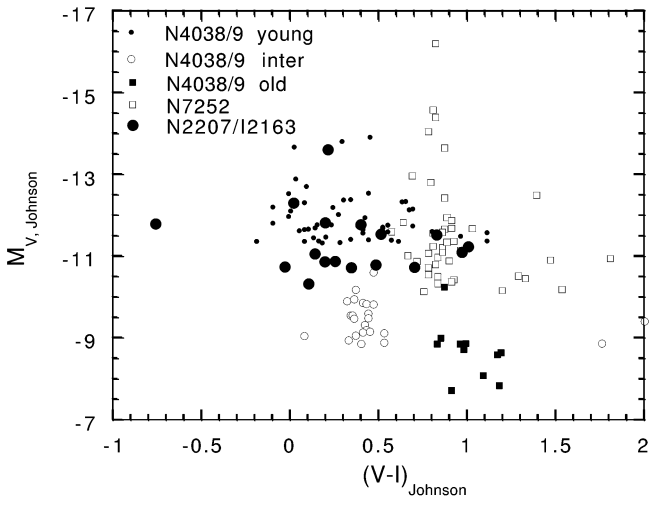

FIG. 13.—Color-magnitude diagram for SSCs in IC 2163 and NGC 2207 (*large filled circles*) compared with SSCs measured by Whitmore et al. (1999) in the Antennae (N4038/9), including young SSCs (*small filled circles*), intermediate-age SSCs (*open circles*), and old SSCs (*filled squares*), and SSCs measured by Miller et al. (1997) in NGC 7252 (*open squares*). All measurements are shown on the Johnson scale. The SSCs in IC 2163 and NGC 2207 resemble the young population in the Antennae and those in NGC 7252.

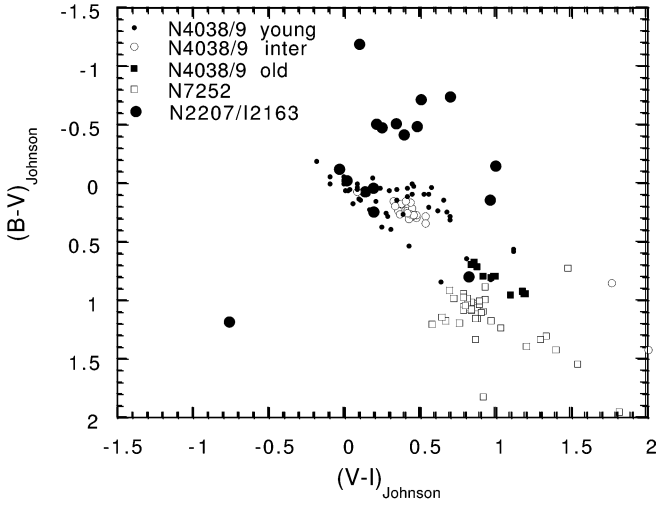

FIG. 14.—Color-color diagram for SSCs in IC 2163 and NGC 2207, the Antennae, and NGC 7252. Coding is the same as in Fig. 13. The SSCs in IC 2163 and NGC 2207 have similar $V-I$ colors as the other galaxies but bluer $B-V$ colors.

10^8 yr. The masses of the SSCs are typically a few times 10^4 $M_\odot$ for the younger ages or as much as a factor of 3 higher for older ages. These are smaller by a factor of ~ 10 than those of the SSCs in the other galaxies mentioned previously. The magnitudes, colors, and masses (for the younger ages, if the colors are double-valued) are listed in Table 2 for each of our SSCs.

SSCs can form during the strong interaction between two galaxies. For example, in the Antennae, the star formation rate is very large and there are $\sim 10^3$ SSCs, some near the edges of the overlap region and others in the western loop (Whitmore et al. 1999). Less active galaxies have SSCs too. The controlling parameter seems to be the overall star formation rate per unit area (Larsen & Richtler 2000). According to Larsen & Richtler, the interaction itself does not favor the production of SSCs, it only promotes a high star formation rate, and then the SSC fraction is determined by this rate. To compare our SSC population with the correlation found by Larsen & Richtler (2000), we summed the U-band luminosities of the 15 SSCs belonging to NGC 2207 in their Table 7 (clusters 3–17) and divided by the U-band luminosity of the whole galaxy. The result is 0.16%. We also determined the star formation rate per unit area from the far-infrared (FIR) flux and D_0 in the RC3, following equation (7) in Larsen & Richtler. Because IRAS could not resolve the two galaxies separately, the FIR flux given in the RC3 is the sum of each. We take 0.6 times this FIR flux to represent NGC 2207, based on the ratio of near-infrared (NIR) fluxes. This yields $2 \times 10^{-3}\ M_\odot\ \mathrm{yr}^{-1}\ \mathrm{kpc}^{-2}$. For this star formation rate, Larsen & Richtler would predict a relative SSC U-band luminosity in the range 0.5%–1% for clusters more massive than $3 \times 10^4\ M_\odot$, instead of our relative luminosity of 0.17%. Thus we have too few SSCs. This disagreement is not surprising, considering our assumptions and the difficulty of finding SSCs in NGC 2207 and also the different telescopes and spatial resolutions for the two studies. Nevertheless, the number of SSCs in NGC 2207 is not particularly unusual, so we cannot conclude that the interaction triggered the formation of these SSCs directly.

Virtually all the SSCs found here are in regions with high velocity dispersion in the H I gas, typically 50 to 60 km s^{-1} (see Paper II). There are other large regions in these galaxies that have a high velocity dispersion and no SSCs. In NGC 2207, the SSCs are all in the northern half of the galaxy on spiral arms in the outer to middle disk (see Fig. 1). This is the part of NGC 2207 that might have been grazed by the nearside (northern) part of IC 2163, so the interaction could have been important. On the other hand, small number statistics could yield such a lopsided distribution in a random sample.

4.5. *Luminosity Functions for Star-forming Regions*

The luminosity distribution functions for the star-forming regions in each galaxy are shown in Figure 15. The high-luminosity end was fitted to a power law with the form $\log n(M_V) = \text{const} + (0.23 \pm 0.005)M_V$ for NGC 2207 and $\text{const} + (0.34 \pm 0.02)M_V$ for IC 2163. These convert to functions of luminosity, $L \propto 10^{-0.4M_V}$, that have the distributions $n(L)d\log L \propto L^{-\alpha}d\log L$, where $\alpha = 0.58 \pm 0.12$ for NGC 2207 and 0.85 ± 0.05 for IC 2163. Considering the large uncertainties, these luminosity functions for star-forming regions are similar to the cluster luminosity functions in NGC 7252, where $\alpha \sim 0.8$ (Miller et al. 1997), and in the Antennae, where $\alpha \sim 1$ (Zhang & Fall 1999), as well as to those in other galaxies of similar Hubble type (see Elmegreen & Salzer 1999). They are also similar to the H II region luminosity functions in other galaxies (Kennicutt et al. 1989) and in the Milky Way (Williams & McKee 1997), where $\alpha \sim 0.8$–1.

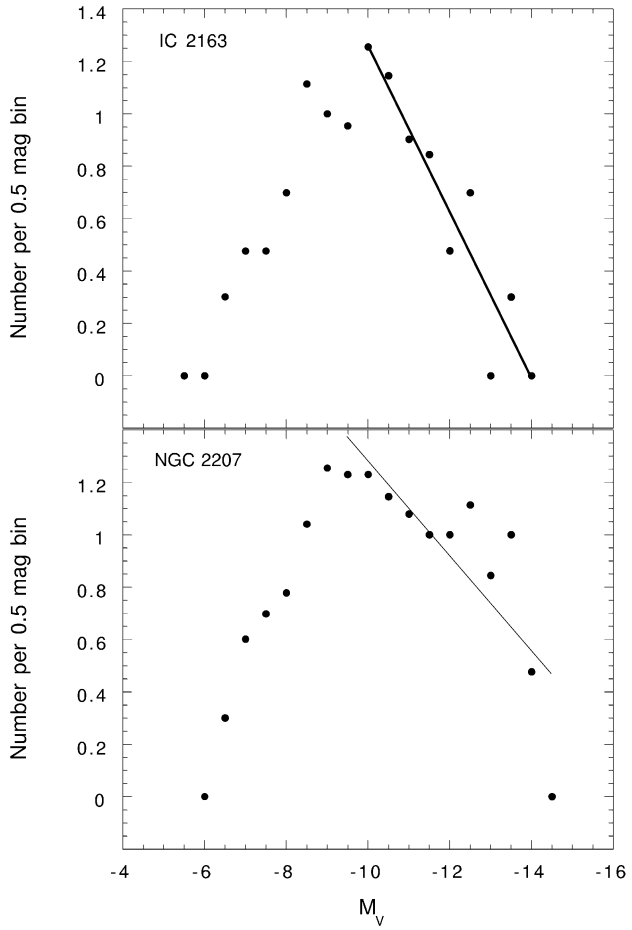

FIG. 15.—Differential luminosity distribution functions for the star-forming regions in IC 2163 and NGC 2207, showing fits to the high-luminosity ends (*lines*). There is incompleteness at the turnovers at fainter than −9.5 mag.

4.6. *Hα Luminosity*

Narrowband Hα and broadband *R* images of IC 2163 and NGC 2207 were obtained by Deidre Hunter with the Lowell 1.1 m telescope on 1999 October 6 for comparison with our optical measurements. The image scale is 1.″1 pixel^{-1}; the pixels were binned 2 × 2. There were four Hα images that were combined to give a total exposure time of 3600 s and three *R*-band images with a total exposure time of 900 s. A scaled *R*-band image was subtracted from the Hα image to remove the continuum; the continuum-subtracted image is shown in Figure 16. The narrow filter width excludes the [N II] line redshifted from 6583 Å but includes the 6548 Å line, whose contamination may contribute as much as 15% of the light for solar metallicity complexes. Hα luminosities were determined based on calibrations of standard stars (Massey et al. 1988) observed during the run.

The total Hα luminosity of IC 2163 is 8.6×10^{40} ergs s^{-1}, compared with 3.1×10^{41} ergs s^{-1} for NGC 2207. Assuming a conversion to a star formation rate $\text{SFR} = 7.07 \times 10^{-42} L_{\text{H}\alpha} M_\odot \text{ yr}^{-1}$ (Kennicutt 1989), these luminosities imply an SFR of 0.61 $M_\odot$ yr^{-1} for IC 2163 and 2.19 $M_\odot$ yr^{-1} for NGC 2207. The cumulative *V*-band luminosity functions of the star-forming regions in § 4.6 also imply that the total young star luminosity of IC 2163 is about 30% of that in NGC 2207, whereas the NIR luminosity ratio is 60%. The average SFR in a galaxy disk is a function of its Hubble type and mass. The total H I masses for IC 2163 and NGC 2207 are 4.8×10^9 $M_\odot$ and 2.2×10^{10} $M_\odot$ (Paper I). Scaled to an H I mass of 10^{10} $M_\odot$, their SFR would be 1.27 and 1.00 $M_\odot$ yr^{-1}, respectively. For typical Sc galaxies such as IC 2163, the SFR for an H I mass of 10^{10} $M_\odot$ ranges from 0.2 to 7.0 $M_\odot$ yr^{-1}, with a median value of 1.5 $M_\odot$ yr^{-1} (Ferrini & Galli 1988), so the SFR in IC 2163 is comparable to that in normal noninteracting disks. Similarly, the SFR for Sbc galaxies such as NGC 2207 is 0.03 to 1.5 $M_\odot$ yr^{-1} per 10^{10} $M_\odot$, with a

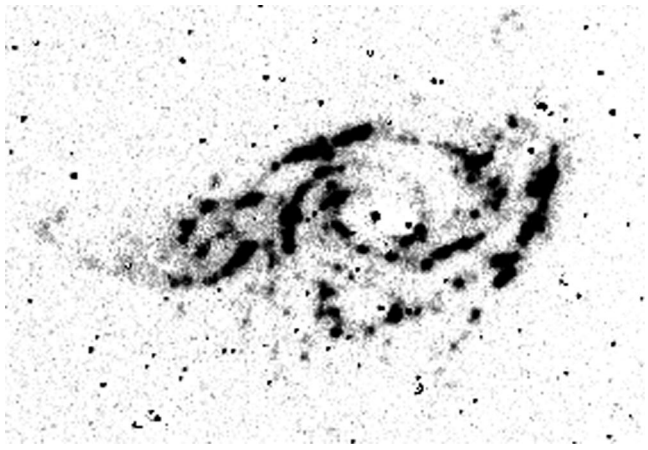

FIG. 16.—Hα continuum-subtracted image of IC 2163 and NGC 2207, based on images obtained by D. Hunter with the Lowell 1.1 m telescope. The Hα peaks are generally coincident with the star-forming regions measured from the *HST* images; the brightest peak, in the far western arm of NGC 2207, coincides with a strong radio continuum source.

median value of 0.4 $M_\odot$, so the SFR in NGC 2207 is also normal.

Hα fluxes were measured for 59 large-scale star-forming regions, whose diameters range from 400 to 1600 pc. Twelve regions measured in the inner spiral arms and eyelids of IC 2163 account for 30% of its total Hα luminosity. The inner spiral arms of NGC 2207 account for about 10% of the total Hα luminosity from that galaxy, with the outer spiral arm regions accounting for 29% of the total. The largest, most luminous H II region in Figure 16 is associated with the nonthermal radio source (discussed in Paper III) on the outer western arm of NGC 2207; this region also contains a supernova remnant and the optically thick dark cloud discussed in § 3.

The luminosity function for H II regions is shown in Figure 17. The slope at the high-luminosity end is -0.7 ± 0.2, which is consistent with the slope found for star-forming regions above and for H II regions in normal spiral disks (Kennicutt et al. Hodge 1989; Elmegreen & Salzer 1999). Figure 18 plots the logarithm of the diameter of the H II regions as a function of the logarithm of the Hα luminosity. A bivariate fit yields the relation $\log L_{\mathrm{H}\alpha} \approx (30.6 \pm 1.1) + (3.0 \pm 0.4) \log D$. There is no significant difference between the H II regions in IC 2163 and NGC 2207, which is consistent with the *HST* results for star clusters.

A high-resolution Canada-France-Hawaii Telescope Hα study of the metallicities of the two galaxies is in progress by P. Martin. Several of the large star-forming regions that we see on Hunter's image taken with the Lowell 1.1 m telescope are resolved into smaller units on his image.

4.7. *Red Stars in the Field*

Numerous red starlike objects appear all over the field of the two galaxies; they are not all necessarily associated with the galaxy pair, however. Photometric fits to the stellar objects yield Gaussian dispersions of ~1 pixel, which makes them indistinguishable from foreground stars.

Figure 19 shows a two-color diagram with the $B-V$ and $V-I$ colors of several *HST* red stellar objects denoted by open or filled circles (open for those that are on the lines of sight to the two galaxies, and filled for those that are projected against the black sky) and the colors of white dwarfs

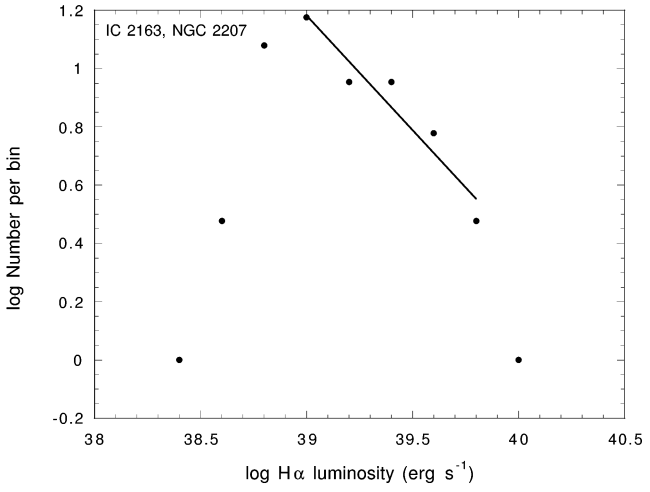

FIG. 17.—Differential luminosity distribution function for H II regions in IC 2163 and NGC 2207, with a fit (*line*) to the high-luminosity end. The fit is similar to that for galaxies with these Hubble types.

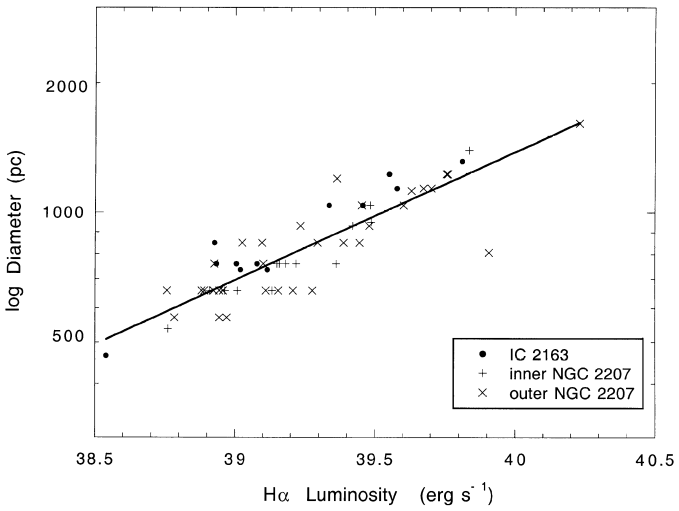

FIG. 18.—Diameter vs. logarithm of Hα luminosity for IC 2163 (*circles*), H II regions in the inner parts of NGC 2207 (*plus signs*), and H II regions in the outer parts of NGC 2207 (*crosses*). A bivariate least-square fit is shown as a line for all the regions.

(Bergeron, Wesemael, & Beauchamp 1995), Milky Way globular clusters (Harris 1996), and normal stars in various luminosity classes denoted by other symbols (from Straizys 1992). According to the two-color diagram, the *HST* objects could be any type of star, including a white dwarf, or they could be distant old globular clusters.

Figure 20 shows the *absolute V* magnitudes for various objects, plotted versus the $V-I$ color. For the *HST* objects, the *apparent V* magnitudes are plotted. This diagram shows what distances have to be used for the *HST* objects to be a particular type of object. The right-hand axis shows how far the objects would have to be from us for their apparent magnitude of 21 to correspond to a given absolute magnitude. On the basis of this diagram, the *HST* field stars could be main-sequence stars at 2–5 kpc, pre–main sequence stars

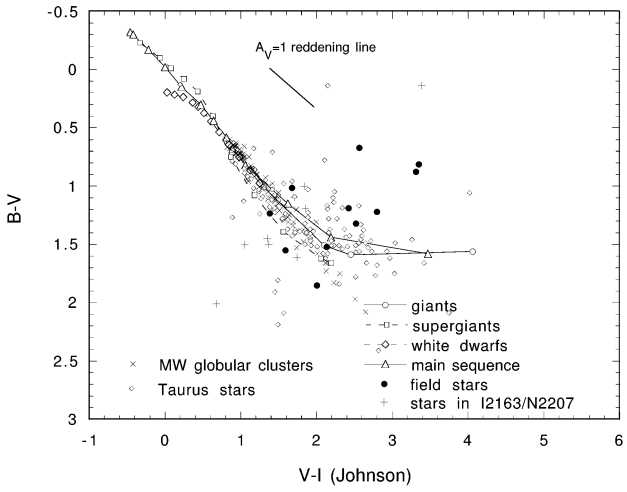

FIG. 19.—Color-color diagram for the red stars in the field of view of the two galaxies (filled circles outside the main optical boundaries of the galaxies are "field stars"; plus signs inside their boundaries are stars in IC 2163 and NGC 2207). For comparison, colors for several types of stars are also shown, as well as globular clusters in the Milky Way and stars in Taurus. The curved line represents the main sequence; the straight line indicates the shift corresponding to 1 mag of visual extinction.

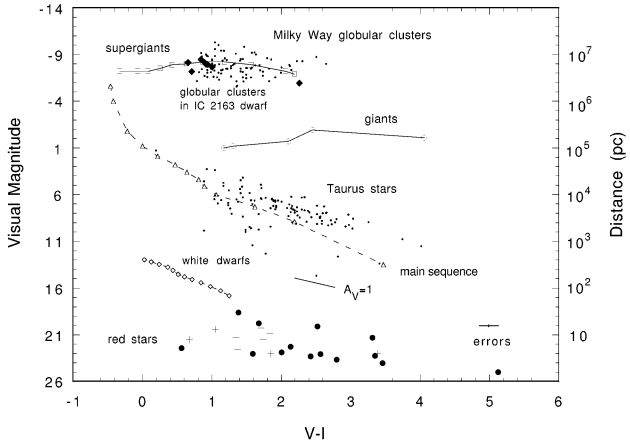

FIG. 20.—Color-magnitude diagrams for red stars in the field of the two galaxies and for other types of stars, with the same coding as in Fig. 19. All magnitudes are absolute except those for the red field stars, which are apparent magnitudes. The right-hand vertical axis represents the distance from us to the red star for it to have a given absolute magnitude. Most likely, the red field stars are main-sequence stars at a distance of 2–5 kpc. Absolute magnitudes are also shown for globular clusters in the dwarf galaxy in the eastern tidal arm IC 2163, assuming a distance of 35 Mpc.

at 5–10 kpc, giants at ~100 kpc, or either supergiants or globular clusters such as the Milky Way globulars at ~8 Mpc. This latter match might include globular clusters at the 35 Mpc distance of IC 2163/NGC 2207 if the *HST* field objects are the brightest members of this class of objects and they are ~20 times brighter than the average Milky Way globular cluster.

There are no known star-forming regions at 5–10 kpc in this direction, which corresponds to galactic coordinates $(l, b) = (228.^\circ7, -17.^\circ0)$. Orion is close to this line of sight, but the *HST* red stellar objects are much too faint for the Orion pre–main sequence. Very old brown dwarfs do not look like a reasonable possibility either if they follow the extrapolation of the red, low-luminosity end of the main sequence (Baraffe et al. 1998). Old halo white dwarfs (Ibata et al. 1999) are not a likely explanation because they are too blue in $V-I$. Also, the objects in the *HST* field would have to be more than 10 times closer than halo white dwarfs, because their apparent magnitudes are ~24 mag. Most likely, these objects are field main-sequence stars at 2–5 kpc and are typically located a few scale heights above the galactic midplane.

5. NUCLEAR REGION OF IC 2163

The center of IC 2163 contains a bright, clumpy nuclear disk with diameter $5''.25 = 0.9$ kpc. It is crossed by intricate dust structure, partly from foreground obscuration by NGC 2207; a dust streamer divides the central maximum from a second bright region ~1″.4 to its east. An irregular ring of dust partially surrounds the nuclear disk. In the south and east, it is a continuation of the inner western spiral arm dust lane. Figure 21 (*left*) shows a Planetary Camera V-band image, while Figure 21 (*right*) shows the B-band contours overlaid on a $B-I$ map. These figures are rotated 10.°7 clockwise relative to absolute coordinates.

On the assumption that the nuclear disk is intrinsically circular, the values for its apparent axis ratio and orientation are a nice confirmation of the orientation parameters found for IC 2163 in Papers I and II. In the sky plane, the nuclear disk has an axis ratio of $3''.75/5''.25 = 0.71$ and major axis position angle $61^\circ \pm 2^\circ$ (this is after correction for the rotation of the above figure). This axis ratio implies an inclination of 45° if the disk is intrinsically circular. Papers I and II found a position angle of $65^\circ \pm 10^\circ$ for the projection line of nodes of the galaxy and an inclination of $40^\circ \pm 5^\circ$. These values differ from the apparent position angle and inclination of the outer optical disk because the outer disk is intrinsically oval.

The central 1″ region (190 pc) measured on the *HST* PC images has colors of $U-B = 0.52$, $B-V = 1.13$, and $V-I = 1.52$, with brightness $M_B = -13.29$. For comparison, Frogel (1985) measured very similar colors for the nucleus of NGC 2207 in a 6″.6 region from ground-based observations: $U-B = 0.57$, $B-V = 1.00$.

The extinction corrections in the entire nuclear region of IC 2163 are uncertain and vary from region to region. There are several prominent dust clumps on the eastern side of the nuclear region; the magnitude differences relative to their surrounding regions range from 0.5 to 1.5 mag in V band. A comparison of the radial profiles in the nucleus on the east and west sides also indicates about 1.2 mag more extinction in V band on the eastern side. If we assume that the foreground obscuration is $A_V \sim 1$ mag for the dust lane

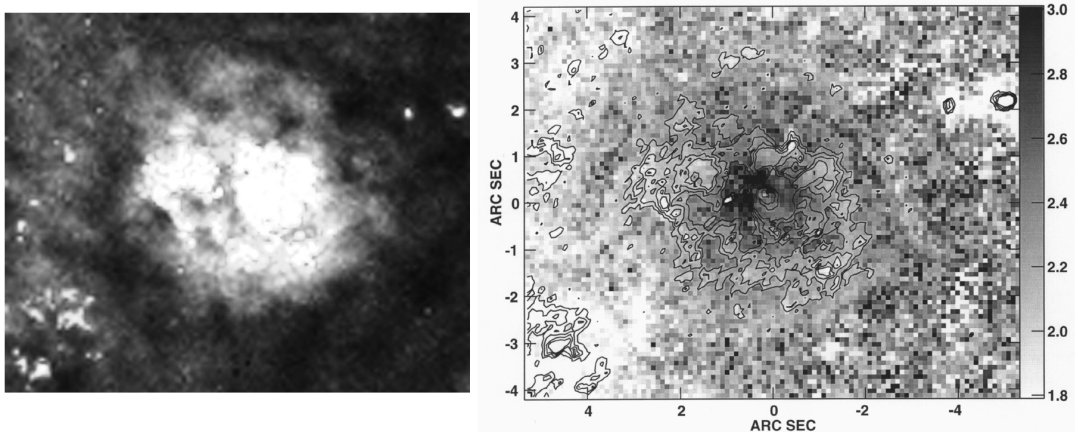

FIG. 21.—*Left*: PC image of the nuclear region of IC 2163 in V band. The field of view is approximately 10″. *Right*: $B-I$ image of the same region, shown on a gray scale, with B-band contours overlaid and coordinates marked.

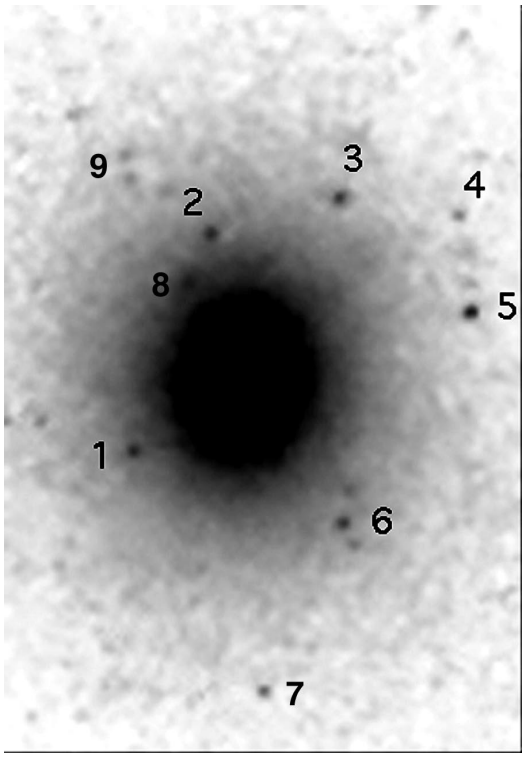

FIG. 22.—Globular clusters in the dwarf galaxy in the eastern tidal arm of IC 2163, indicated by numbers on this V-band image.

streamers from NGC 2207 in the central 1″ of IC 2163, then the extinction-corrected colors are $B-V = 0.81$ and $V-I = 1.00$. This $B-V$ color is too red to be attributed to a single starburst any time in the last 10^9 yr. An extinction of $A_V \sim 2-3$ mag could be matched by a single population with an age of about 5 Myr.

Frogel found for the nuclear regions of NGC 2207 and similar late-type spirals that the internal extinction in V band is less than 1.7 mag. After correcting for this extinction, he fitted the observed visible and infrared nuclear colors of the galaxies with three populations of stars having ages of 0.1, a few, and 10 Gyr. We interpret our results for IC 2163 in the same way: there is a combination of old and young stellar populations with no prominent starburst. This result is consistent with the lack of a strong Hα peak in the nucleus (see Fig. 16).

6. POSSIBLE DWARF GALAXY NEAR IC 2163

At the end of the eastern tidal arm of IC 2163, a small uncataloged galaxy with an unknown redshift is visible in Figure 1. We measured its apparent V magnitude to be ~ 17.7, with colors $U-B = 0.43$, $B-V = 0.78$, and $V-I = 1.6$. For comparison, the $B-V$ colors of the elliptical galaxy companions to M31 are 0.74 for NGC 185 and 0.82 for NGC 205 (based on NED[8]).

An ellipse fit for the dwarf yields position angle 183°.7 $\pm 2°$ and an ellipticity of 0.25 that is nearly constant with radius. The center has a bright unresolved nucleus. The radial profile beyond the nucleus is equally well fitted by an exponential and an $r^{1/4}$ law. Thus, the galaxy could be a nucleated dwarf elliptical (dE, N) galaxy or an S0 galaxy. The presence of several apparent old globular clusters in its outer regions suggest that it is a dwarf elliptical galaxy, since it resembles other dE, N galaxies (e.g., Harris 1996).

Photometry on nine of the globular clusters, marked in Figure 22, indicate colors of $V-I = 0.8$ to 1.0 and apparent V magnitudes of 25.4 to 24.3 mag. If these clusters are at the distance to IC 2163 of 35 Mpc, these apparent magnitudes correspond to absolute V magnitudes of -7.4 to -8.5 mag, which is reasonable for globular clusters. The clusters are also shown on the color-magnitude diagram of Figure 20. Thus, it is likely that the dwarf galaxy is associated with the IC 2163/NGC 2207 pair. At a distance of 35 Mpc, the dwarf galaxy's absolute V magnitude is -15.0 and its isophotal radius at 25 mag arcsec^{-2} is ~ 600 pc.

Numerical simulations by Barnes & Hernquist (1992) and Elmegreen, Thomasson, & Kaufman (1993) suggest that dwarf galaxies can form from some interactions, such as the one between IC 2163 and NGC 2207. On the other hand, the presence of the old globular clusters in its outer regions indicate that it probably existed before.

7. CONCLUSIONS

The interacting galaxies IC 2163 and NGC 2207 provide a laboratory for opacity measurements because of their partial overlap. The intercloud regions of NGC 2207 have an average visual extinction of ~ 0.5 to 1 mag on the line of sight at $\sim 0.6\ R_{25}$, and the dust clouds of both NGC 2207 and IC 2163 have approximately ~ 1–2 mag of visual extinction.

Seventeen star-forming regions with stellar profiles are compact and massive, like super–star clusters found in other galaxies. Eight are in the northern spiral arm of NGC 2207 and two are in the eyelid of IC 2163. Their masses range from $10^4\ M_\odot$ to $2 \times 10^5\ M_\odot$, and their ages from 10^6 to 10^7 yr. According to the correlation found by Larsen & Richtler (2000), the number of SSCs is not unusual for the measured total star formation rates, so it is unclear whether the interaction had anything to do with the formation of these dense clusters.

The large-scale star-forming regions in both galaxies have normal luminosity-size distributions and luminosity functions. The star-forming regions in the inner arms and the eyelids of IC 2163 and in the inner arms of NGC 2207 are similar in luminosity and color to those in the rest of the system. The majority of the measured clusters have ages of a few times 10^6 yr, with masses ranging from $10^3\ M_\odot$ to almost $10^6\ M_\odot$. The star formation rates per unit mass in each galaxy, based on the Hα observations, are similar to those of normal spiral disks in the same Hubble type. We conclude that the interaction of the two galaxies has not led to unusual star formation.

The authors gratefully acknowledge support for this work provided by NASA through grant number GO-06483-95A from the Space Telescope Science Institute, which is operated by the Association of Universities for Research in Astronomy, Inc., under NASA contract NAS 5-26555. We thank Deidre Hunter for kindly obtaining the Hα images. D. M. E. thanks Vassar College for partial support from a research grant.

[8] The NASA/IPAC Extragalactic Database (NED) is operated by the Jet Propulsion Laboratory, California Institute of Technology, under contract with the National Aeronautics and Space Administration.

REFERENCES

Baraffe, I., Chabrier, G., Allard, F., & Hauschildt, P. H. 1998, A&A, 337, 403
Barnes, J. E., & Hernquist, L. 1992, Nature, 360, 715
Bergeron, P., Wesemael, F., & Beauchamp, A. 1995, PASP, 107, 1047
Berlind, A., Quillen, A. C., Pogge, R. W., & Sellgren, K. 1997, AJ, 114, 107
Blaauw, A. 1964, ARA&A, 2, 213
Bohlin, R. C., Savage, B. D., & Drake, J. F. 1978, ApJ, 224, 132
Burstein, D., & Heiles, C. 1982, AJ, 87, 1165
de Vaucouleurs, G., de Vaucouleurs, A., Corwin, H. G., Jr., Buta, R. J., Paturel, G., & Fouque, P. 1991, Third Reference Catalogue of Bright Galaxies (New York: Springer) (RC3)
Disney, M., Davies, J., & Phillipps, S. 1989, MNRAS, 239, 939
Domingue, D. L., Keel, W. C., & White, R. E. 2000, ApJ, submitted
Donner, K. J., Engström, S., & Sundelius, B. 1991, A&A, 252, 571
Efremov, Y. 1995, AJ, 110, 2757
Elmegreen, B. G. 1996, ApJ, 467, 579
———. 1997, ApJ, 477, 196
Elmegreen, B. G., & Efremov, Y. N. 1997, ApJ, 480, 235
Elmegreen, B. G., Efremov, Y. N., Pudritz, R. E., & Zinnecker, H. 2000a, in Protostars and Planets IV, ed. V. G. Mannings, A. P. Boss, & S. S. Russell (Tucson: Univ. Arizona Press)
Elmegreen, B. G., et al. 1998, ApJ, 503, L119
Elmegreen, B. G., & Falgarone, E. 1996, ApJ, 471, 816
Elmegreen, B. G. et al. 2000b, AJ, 120, 630 (Paper III)
Elmegreen, B. G., Sundin, M., Kaufman, M., Brinks, E., & Elmegreen, D. M. 1995a, ApJ, 453, 139 (Paper II)
Elmegreen, B. G., Thomasson, M., & Kaufman, M. 1993, ApJ, 412, 90
Elmegreen, D. M. 1980, ApJS, 43, 37
Elmegreen, D. M., Kaufman, M., Brinks, E., Elmegreen, B. G., & Sundin, M. 1995b, ApJ, 453, 100 (Paper I)
Elmegreen, D. M., & Salzer, J. J. 1999, AJ, 117, 764
Elmegreen, D. M., Sundin, M., Elmegreen, B. G., & Sundelius, B. 1991, A&A, 244, 52
Ferrini, F., & Galli, D. 1988, A&A, 195, 27
Fritze-von Alvensleben, U. 1999, A&A, 342, L25
Frogel, J. A. 1985, ApJ, 298, 528
Gill, A. G., & Henriksen, R. N. 1990, ApJ, 365, L27
Gonzalez Delgado, R. M., & Perez, E. 1997, ApJS, 108, 199
Harris, W. E. 1996, AJ, 112, 1487
Heithausen, A., Bensch, F., Stutzki, J., Falgarone, E., & Panis, J. F. 1998, A&A, 331, L65
Hodge, P. 1986, PASP, 98, 1113
Ibata, R. A., Richer, H. B., Gilliland, R. L., & Scott, D. 1999, ApJ, 524, L95
Keel, W. C., & White, R. E., III. 1999, BAAS, 195, 104.05
Kennicutt, R. C. 1989, ApJ, 344, 685
Kennicutt, R. C., Edgar, B. E., & Hodge, P. W. 1989, ApJ, 337, 761
Kennicutt, R. C., & Hodge, P. W. 1980, ApJ, 241, 573
Larsen, S. S., & Richtler, T. 2000, A&A, 354, 836
Larson, R. B. 1992, MNRAS, 256, 641
Leitherer, C., et al. 1999, ApJS, 123, 3 (Starburst 99)
Mandelbrot, B. B. 1983, The Fractal Geometry of Nature (San Francisco: Freeman)
Massey, P., Strobel, K., Barnes, J. V., & Anderson, E. 1988, ApJ, 328, 315
Miller, B. W., Whitmore, B. C., Schweizer, F., & Fall, S. M. 1997, AJ, 114, 2381
Oey, S., & Clarke, C. 1998, AJ, 115, 1543
Pfenniger, D., & Combes, F. 1994, A&A, 285, 94
Rieke, G. H., & Lebofsky, M. J. 1985, ApJ, 288, 618
Rönnback, J., & Shaver, P. A. 1997, A&A, 322, 38
Schlegel, D. 1998, ApJ, 500, 525
Straizys, V. 1992, Multicolor Stellar Photometry (Tucson: Pachart)
Sundin, M. 1989, in Dynamics of Astrophysical Disks, ed. J. A. Sellwood (Cambridge: Cambridge Univ. Press)
Valentijn, E. A. 1990, Nature, 346, 153
Watson, A. M., et al. 1996, AJ, 112, 534
Westpfahl, D. J., Coleman, P. H., Alexander, J., & Tongue, T. 1999, AJ, 117, 868
White, R. E., & Keel, W. C. 1992, Nature, 359, 129
White, R. E., Keel, W. C., & Conselice, C. 1996, New Extragalactic Perspectives in the New South Africa, ed. D. Block & M. Greenberg (Dordrecht: Kluwer)
———. 2000, ApJ, 542, 761
Whitmore, B. C., Zhang, Q., Leitherer, C., Fall, S., Schweizer, F., & Miller, B. W. 1999, AJ, 118, 1551
Williams, J. P., & McKee, C. F. 1997, ApJ, 476, 166
Zhang, Q., & Fall, S. M. 1999, ApJ, 527, L81